Spectroscopy: Optical and Electronic

Spectroscopy is the use of light, sound or particle emission to study matter. It originated through the study of visible light dispersed, according to its wavelength, by a prism. Later, the concept was expanded greatly to comprise any interaction with radiative energy as a function of its wavelength or frequency.

The data that is obtained from spectroscopy is called a spectrum. A spectrum can be used to obtain information about the specimen's energy states, its atomic or molecular arrangements, and related processes.

Nature of the interaction between radiation and material

Types of spectroscopy can be distinguished by the nature of the interaction between the energy and the material.

- Absorption: measuring the fraction of incident energy transmitted through the material.
- Emission: radiative energy released by the material.
- Elastic Scattering: incident radiation reflected or transmitted by a material without energy loss.
- Inelastic Scattering: involving an exchange of energy between the radiation and the matter that shifts the wavelength of the scattered radiation.
- Refraction: the ability of a medium to impede or slow the transmittance of energy.
- Resonance: radiative energy couples two quantum states of the material in a coherent interaction.

Particle nature of photons

Einstein's proposal:

$E = h\nu \Rightarrow P = h/\lambda$

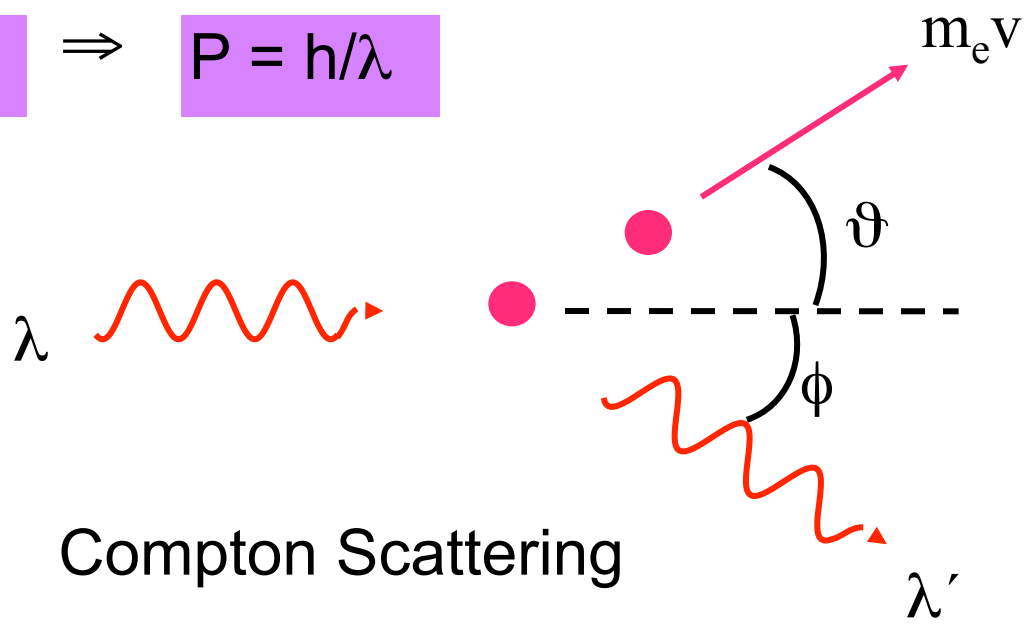

Compton Scattering

Energy levels and bands

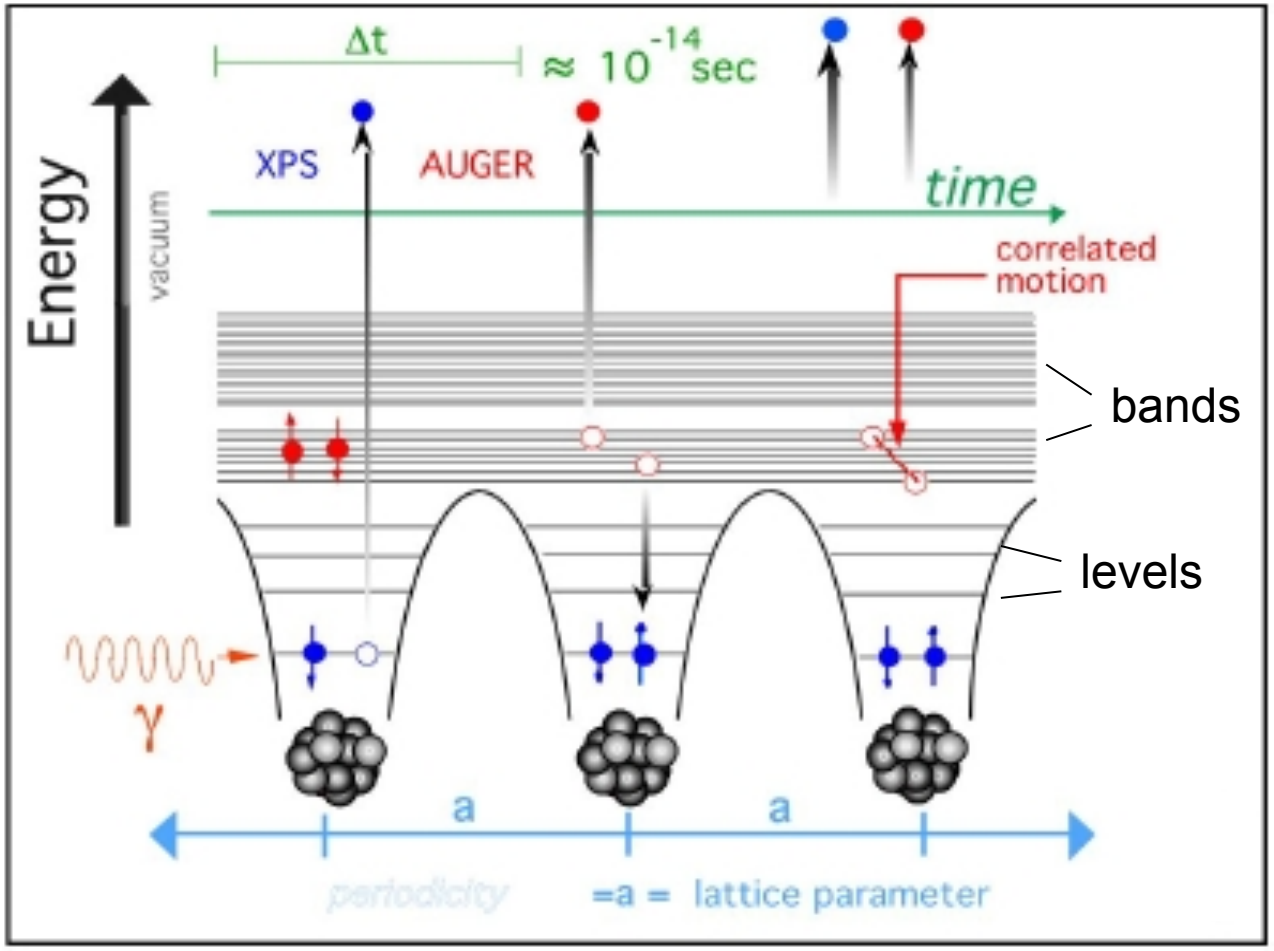

Electronic and vibrational levels

Born-Oppenheimer Approximation

$$\psi_{\text{molecule}}(\vec{r}_i, \vec{R}_j) = \psi_{\text{electrons}}(\vec{r}_i, \vec{R}_j)\psi_{\text{nuclei}}(\vec{R}_j)$$

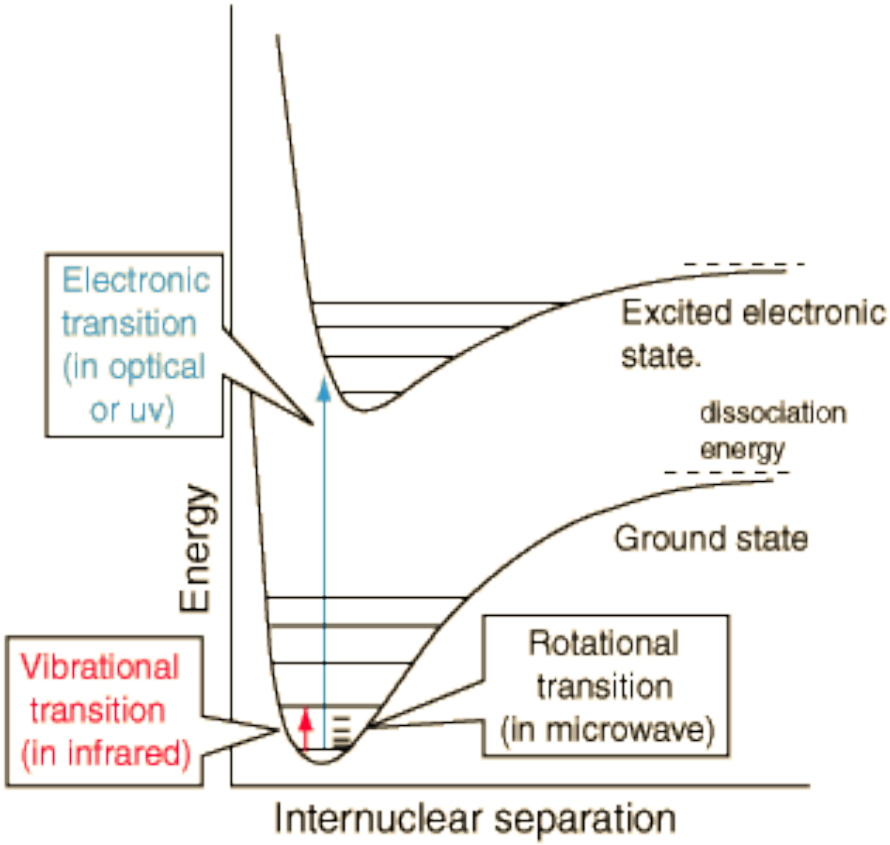

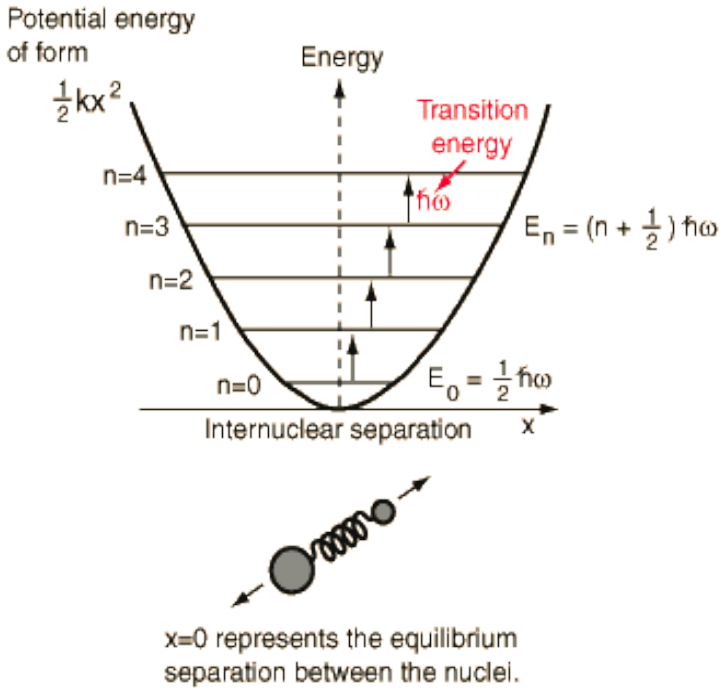

Transition between two quantum states

Fermi's golden rule

Transition rate:

$$T_{i\to f} = \frac{2\pi}{\hbar} \left|\langle f|H'|i\rangle\right|^2 \rho,$$

Transition probability

Density of final states

Transition probability is determined by the wavefunction overlapping of initial and final states, and dictated by the selection rules reflecting the nature of interaction *H'*.

Various spectroscopic methods

Spectroscopy is the use of light, sound or particle emission to study matter.

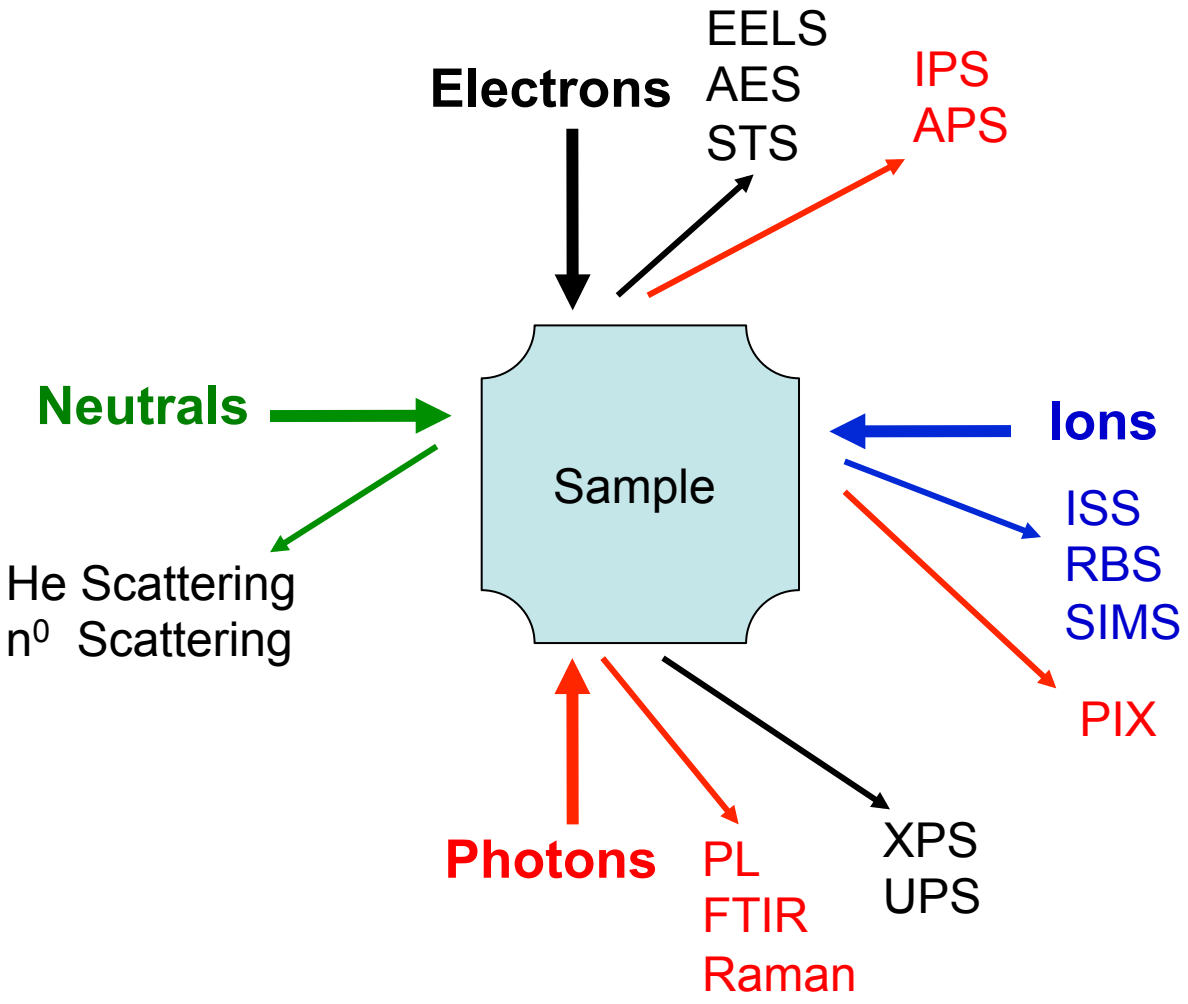

Laser

The term "laser" originated as an acronym for "light amplification by stimulated emission of radiation".

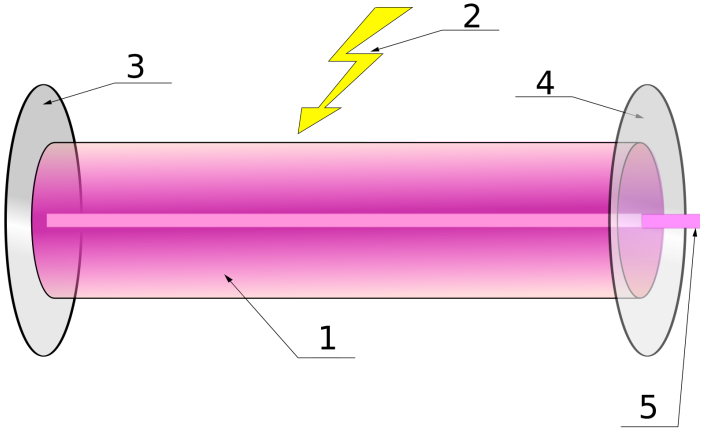

1. Gain medium
2. Laser pumping energy
3. High reflector
4. Output coupler
5. Laser beam

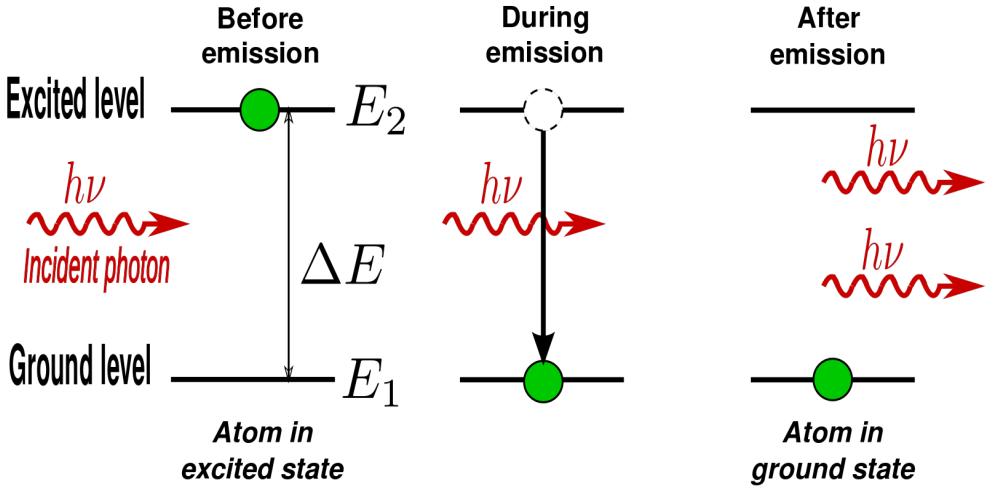

$$E_2 - E_1 = \Delta E = h\nu$$

Types of Lasers

Lasers are commonly designated by the type of lasing material employed, which can be a solid, gas, liquid or semiconductor.

Solid-state lasers have lasing material distributed in a solid matrix (such as the ruby or neodymium:yttrium-aluminum garnet "Yag" lasers). The neodymium-Yag laser emits infrared light at 1,064 nm.

Gas lasers (helium and helium-neon, HeNe, are the most common gas lasers) have a primary output of visible red light. CO_2 lasers emit energy in the far-infrared, and are used for cutting hard materials.

Excimer lasers use reactive gases, such as chlorine and fluorine, mixed with inert gases such as argon, krypton or xenon. When electrically stimulated, a pseudo molecule (dimer) is produced. When lased, the dimer produces light in the ultraviolet range.

Dye lasers use complex organic dyes, such as rhodamine 6G, in liquid solution or suspension as lasing media. They are tunable over a broad range of wavelengths.

Semiconductor lasers, sometimes called diode lasers, are not solid-state lasers. These electronic devices are generally very small and use low power. They may be built into larger arrays, such as the writing source in some laser printers or CD players.

Wavelengths of commercially available lasers

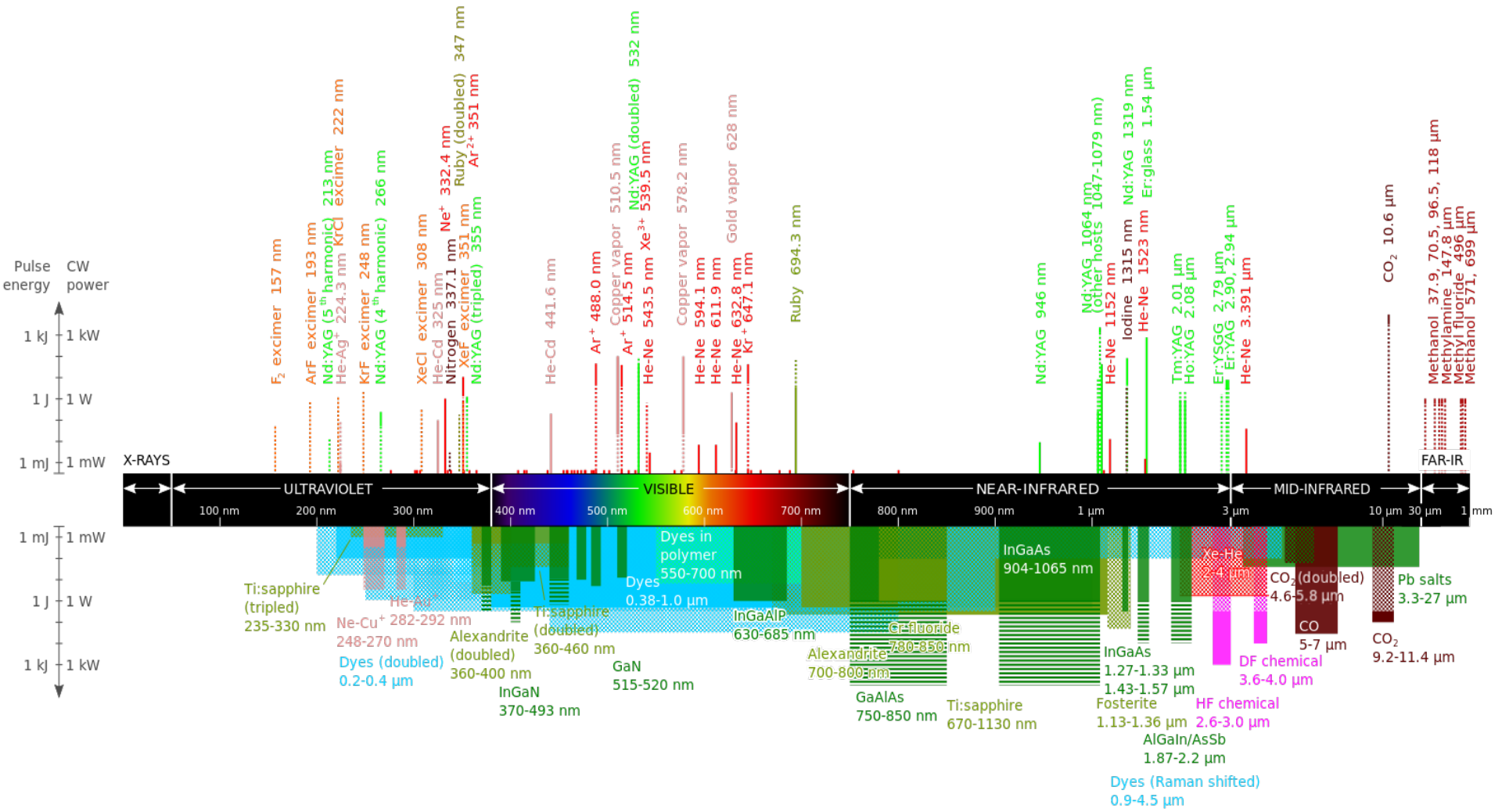

Frequency-doubled green laser pointer

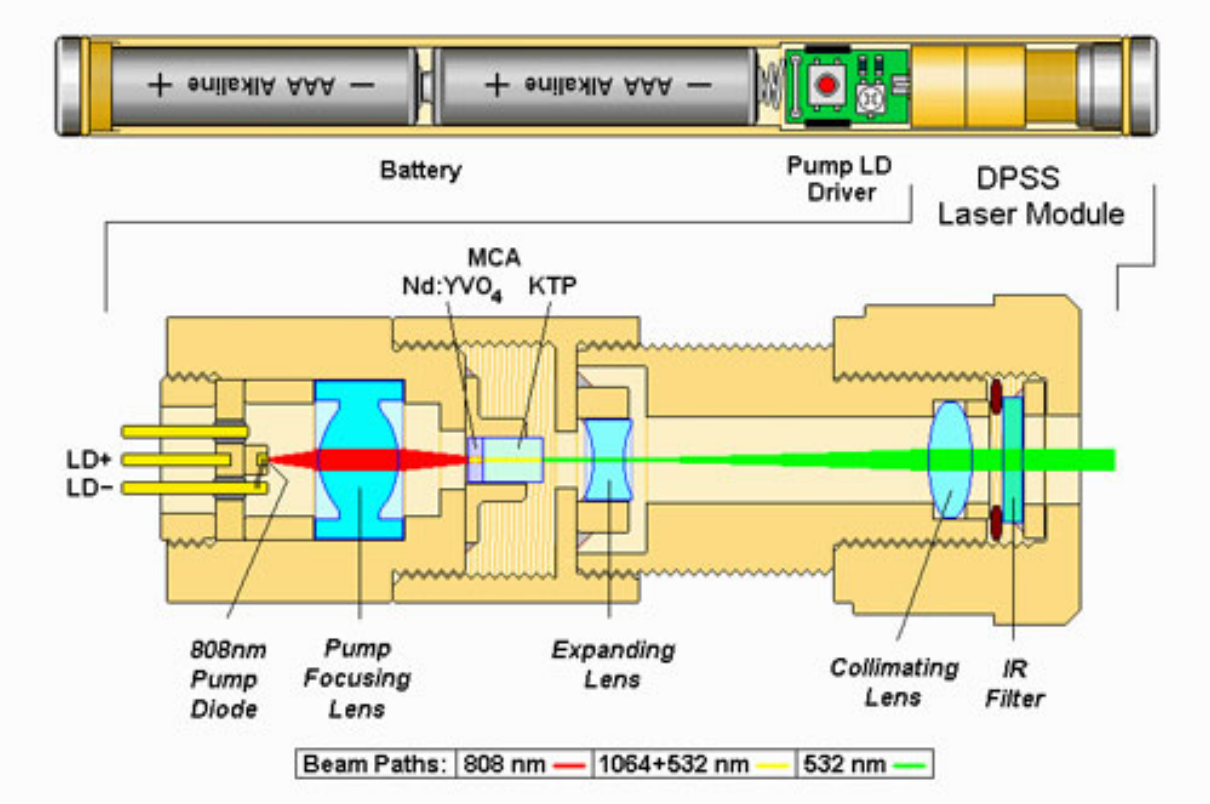

Two AAA cells and electronics power the laser module, which contains a powerful 808 nm IR diode laser that optically pumps a Nd:YVO_4 crystal inside a laser cavity. That laser produces 1064 nm (infrared) light which is mainly confined inside the resonator. Also inside the laser cavity, however, is a non-linear KTP crystal which causes frequency doubling, resulting in green light at 532 nm. The front mirror is transparent to this visible wavelength which is then expanded and collimated using two lenses.

Fluorescence Spectroscopy

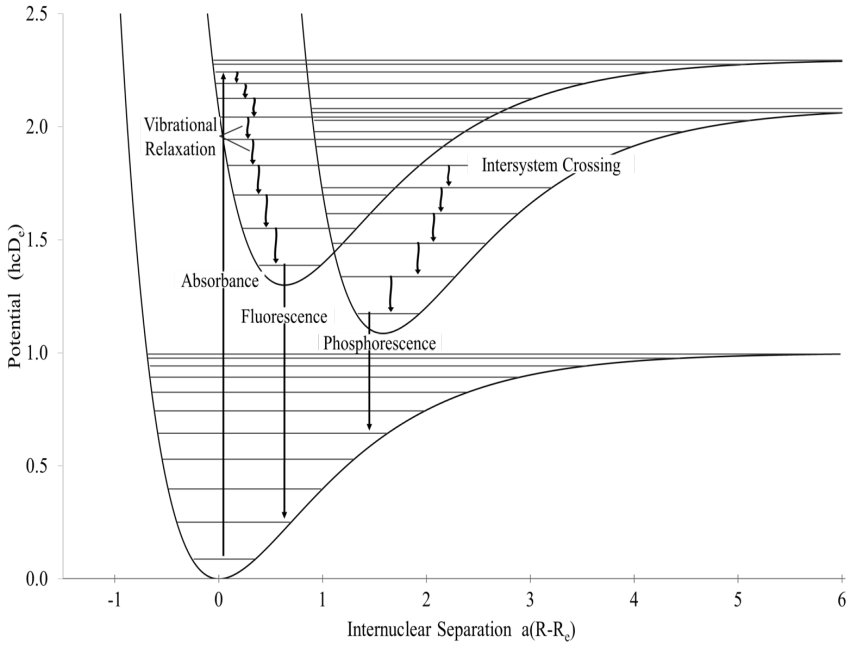

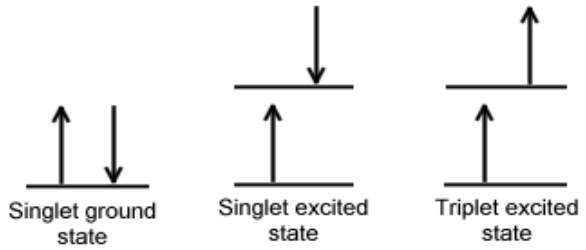

Jablonski Energy Diagram

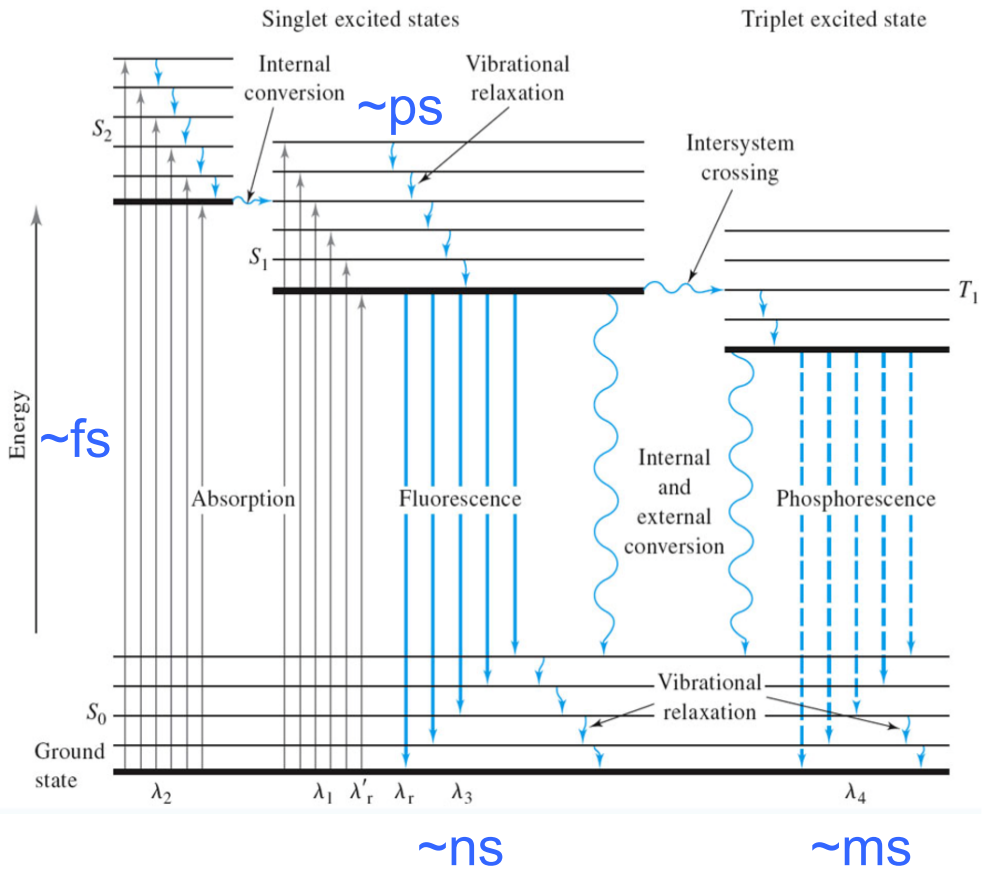

Various Lasers

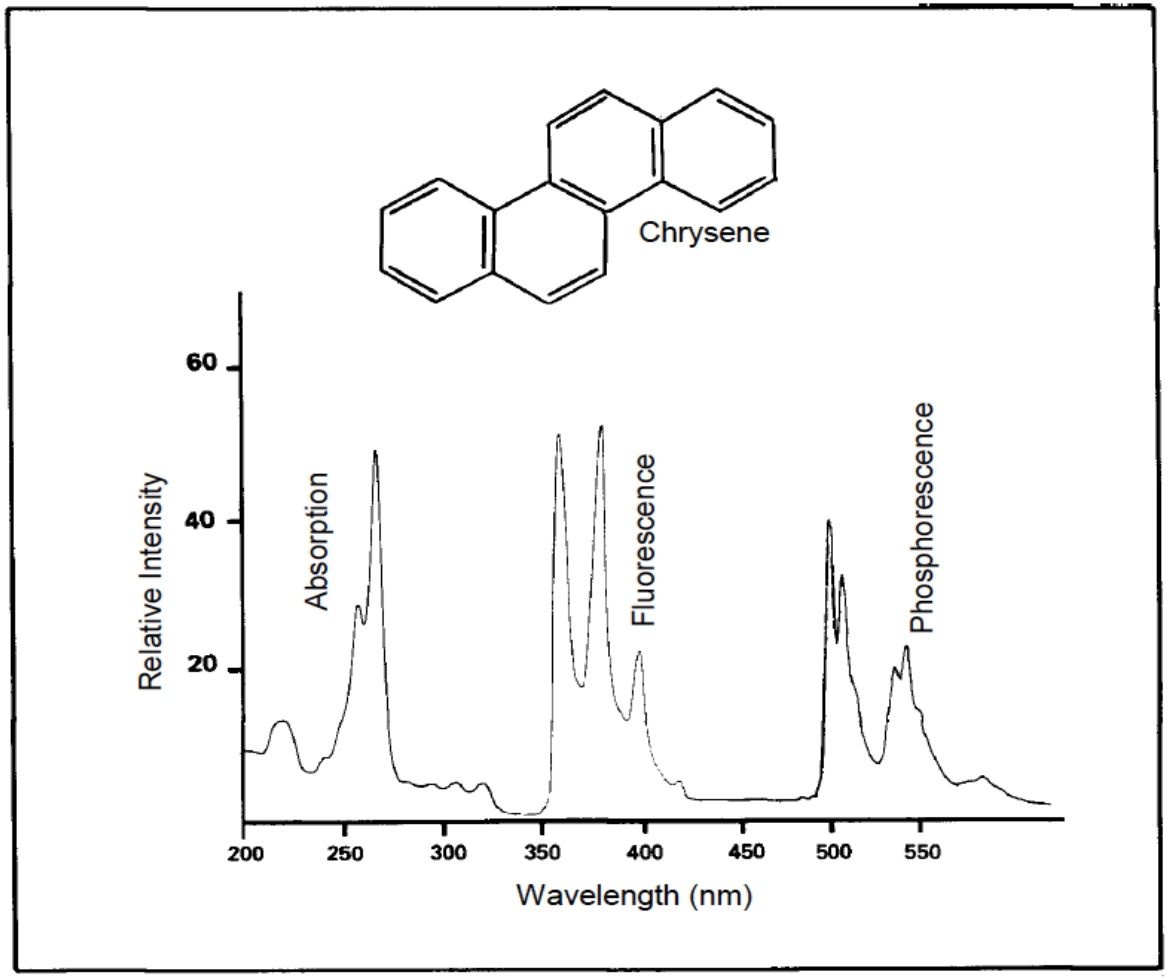

Instrumentation

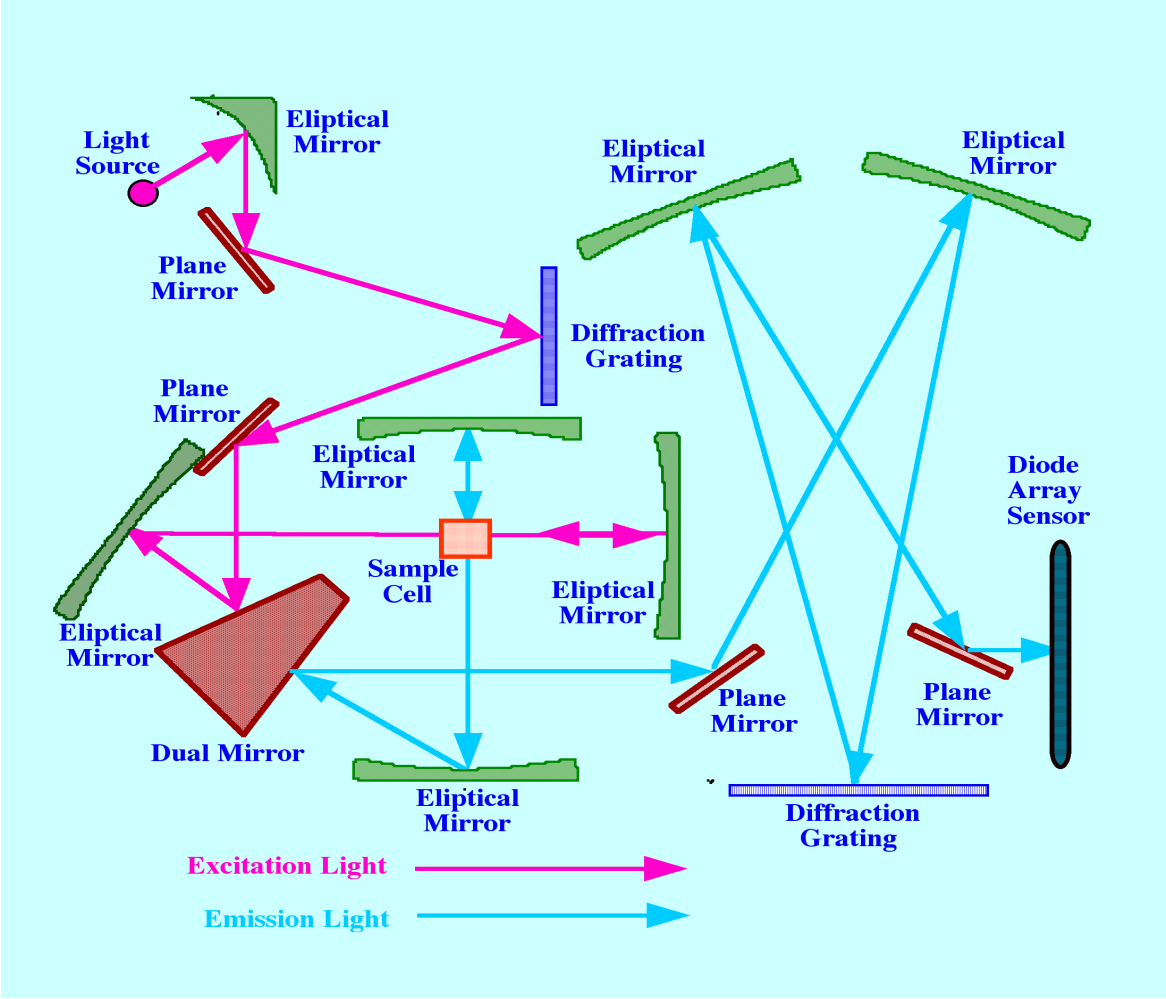

Infrared Spectroscopy

Infrared spectroscopy exploits the fact that molecules absorb specific frequencies that are characteristic of their structure. These absorptions are resonant frequencies.

The infrared portion of the electromagnetic spectrum is usually divided into three regions; the near-, mid- and far- infrared, named for their relation to the visible spectrum. The higher-energy near-IR, approximately 14000–4000 cm^{-1} (0.8–2.5 μm wavelength) can excite harmonic vibrations. The mid-infrared, approximately 4000–400 cm^{-1} (2.5–25 μm) may be used to study the fundamental vibrations and associated rotational-vibrational structure. The far-infrared, approximately 400–10 cm^{-1} (25–1000 μm), lying adjacent to the microwave region, has low energy and may be used for rotational spectroscopy.

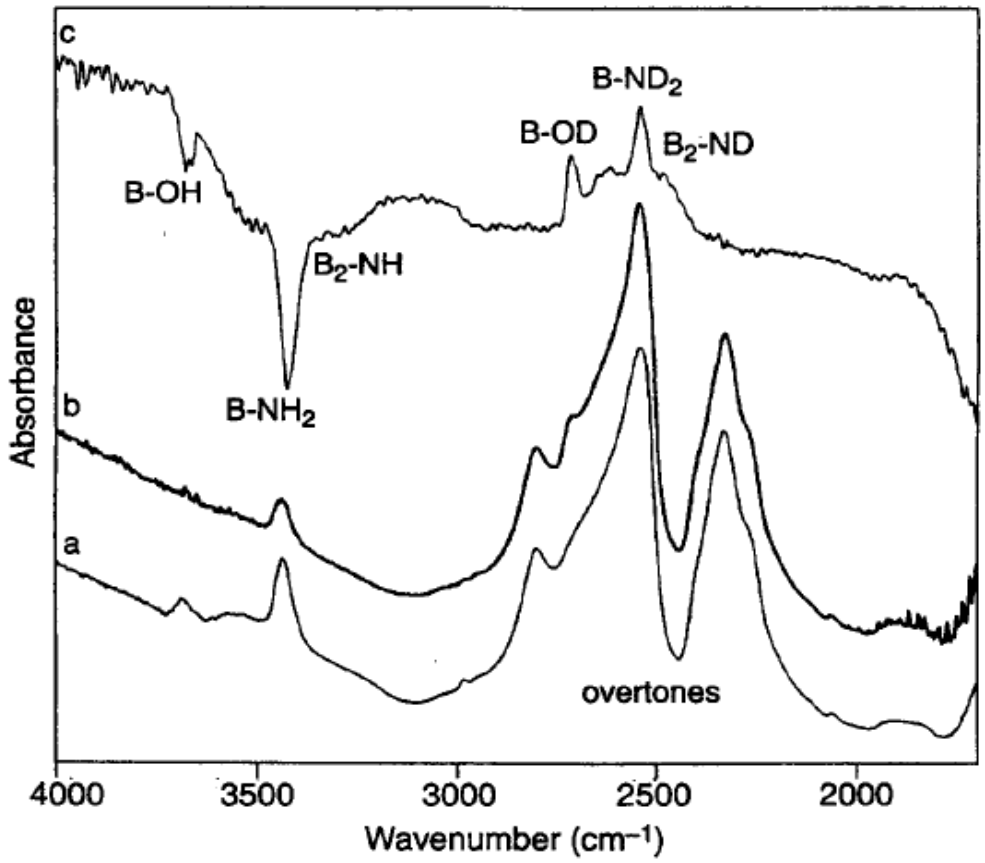

Figure 8.5. FTIR spectra of boron nitride nanopowder surfaces after activation at 875 K (tracing a), after subsequent deuteration (tracing b), and (c) difference spectrum of *a* subtracted from *b* (tracing c). [From M.-I. Baraton and L. Merhari, P. Quintard, V. Lorezenvilli, *Langmuir*, **9**, 1486 (1993).]

Fourier transform infrared spectroscopy (FTIR)

FTIR is a technique which a spectrometer simultaneously collects spectral data in a wide spectral range. This confers a significant advantage over a dispersive spectrometer which measures intensity over a narrow range of wavelengths at a time. FTIR has made dispersive infrared spectrometers all but obsolete.

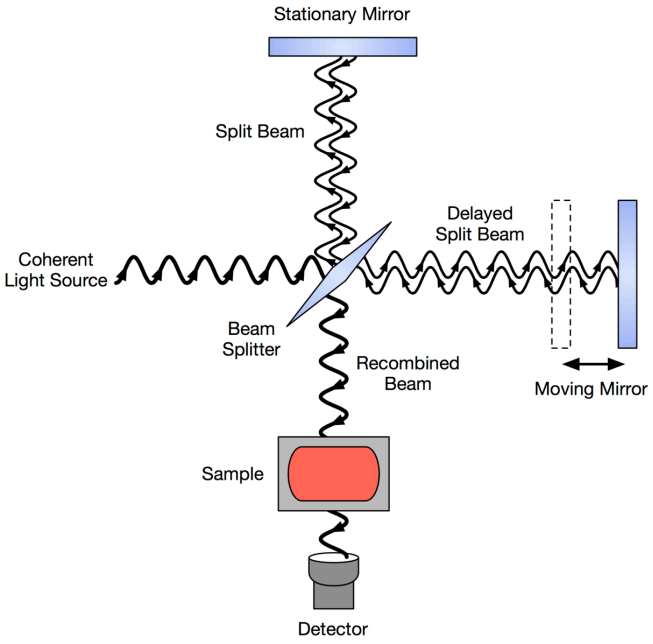

Michelson interferometer

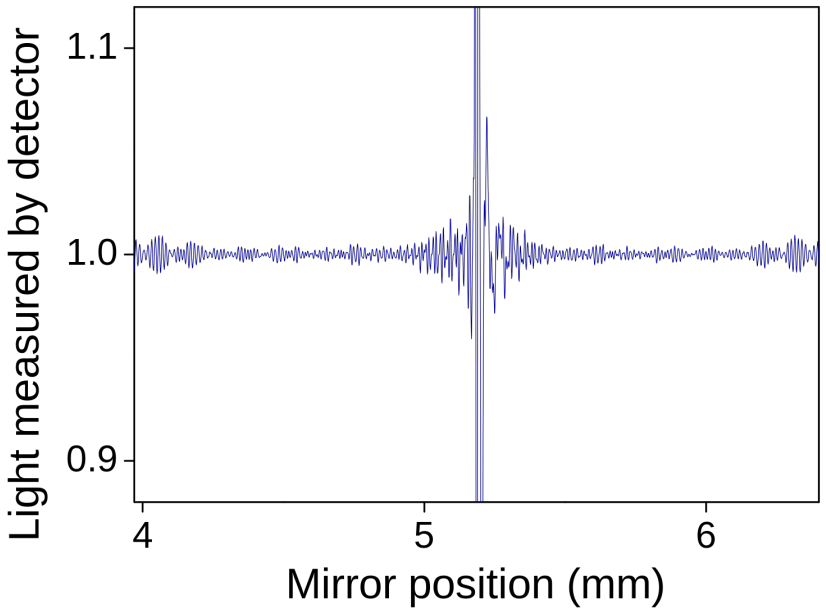

The Theory of Raman Spectroscopy

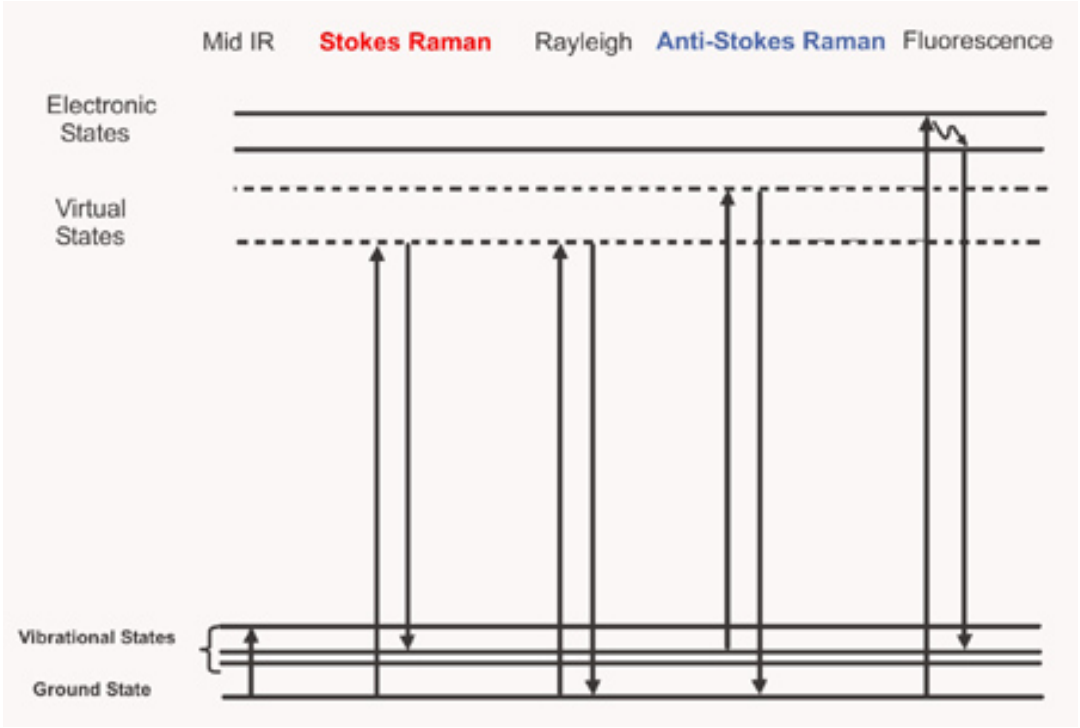

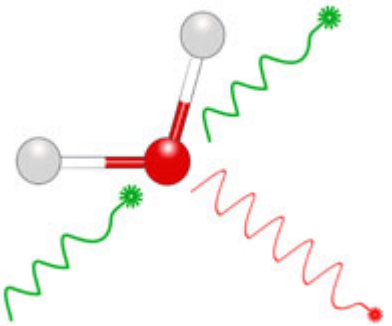

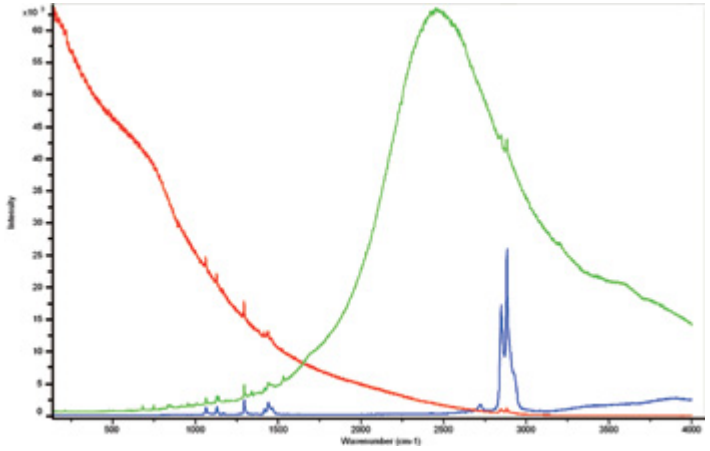

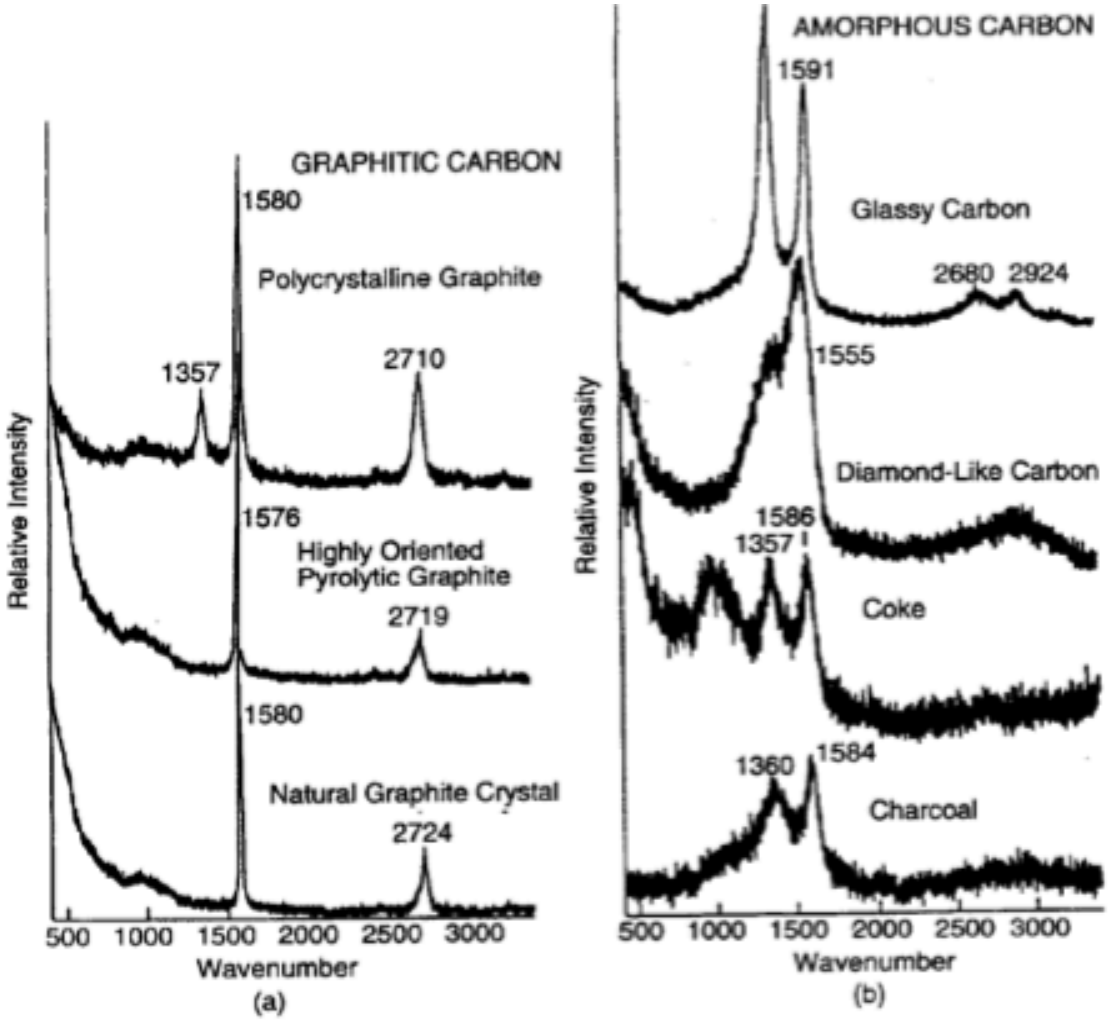

Figure 8.19. Raman spectra of (a) crystalline graphites and (b) noncrystalline, mainly graphitic, carbons. The *D* band appears near 1355 cm^{-1} and the *G* band, near 1580 cm^{-1}. [From D. S. Knight and W. B. White, *J. Mater. Sci.* **4**, 385 (1989).]

X-ray Photoelectron Spectroscopy (XPS)

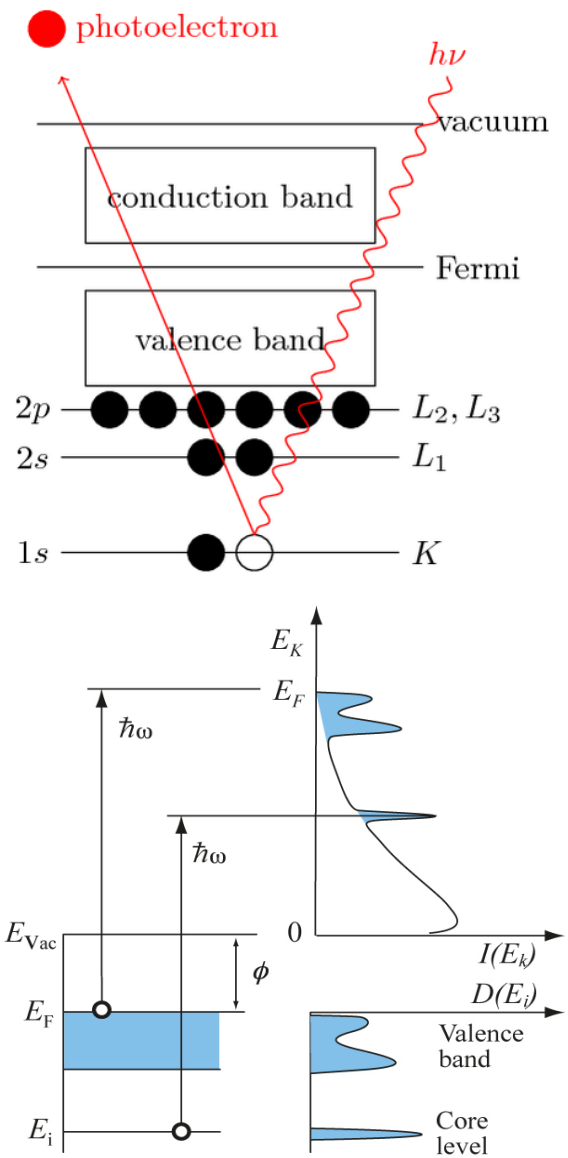

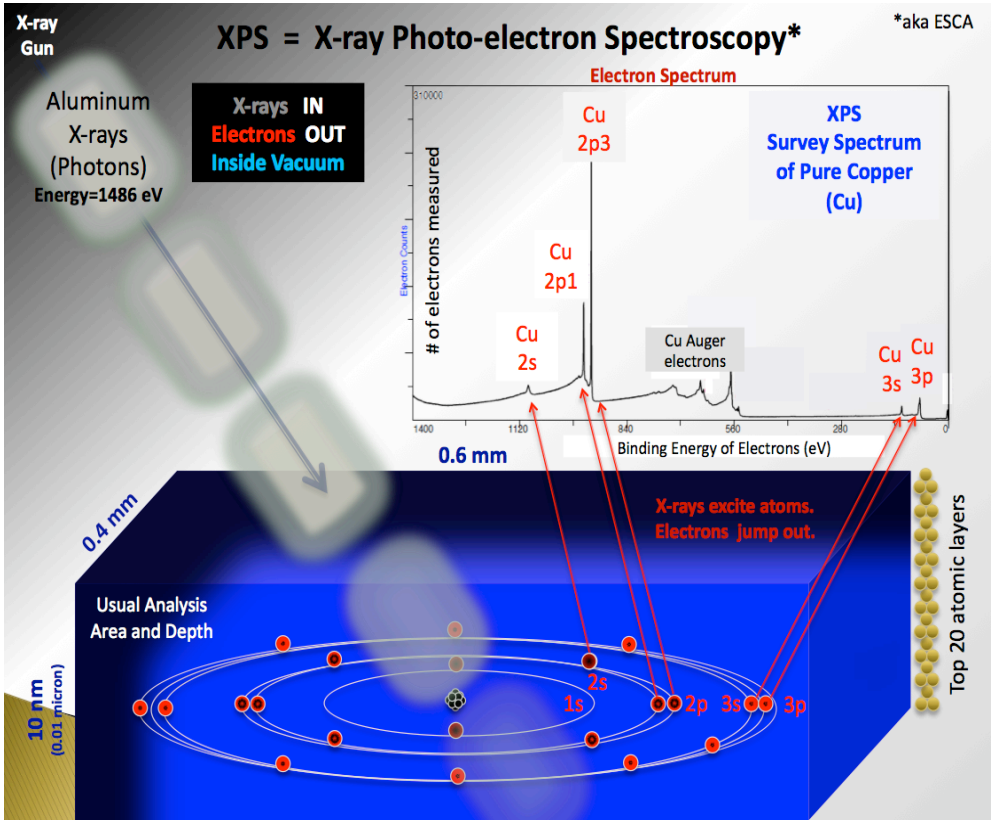

$$E_i = E_{hv} - (E_k + \phi)$$

X-ray source

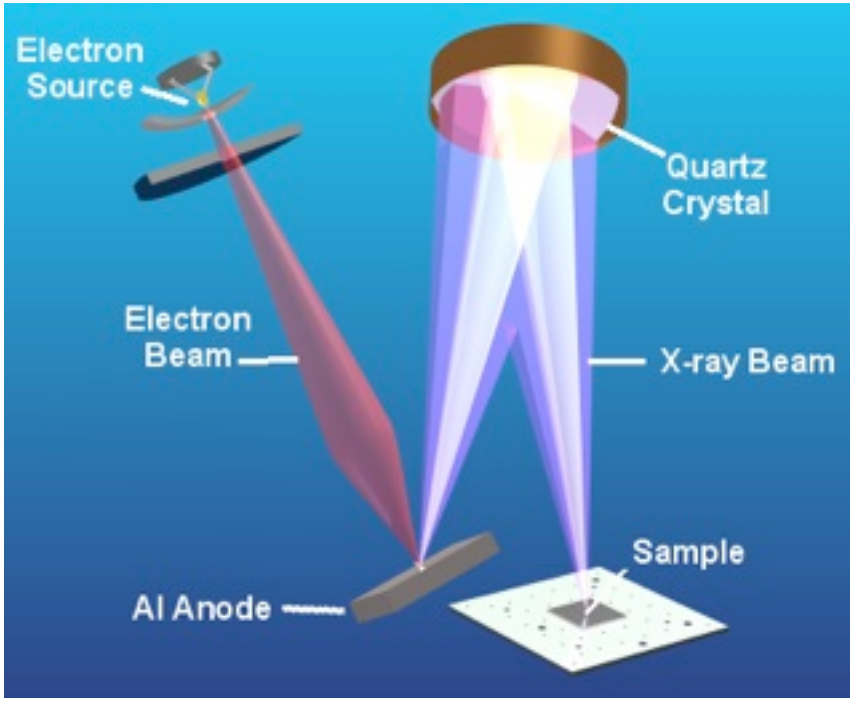
Electron
Source
Quartz
Crystal
Electron
Beam
X-ray Beam
Sample
Al Anode

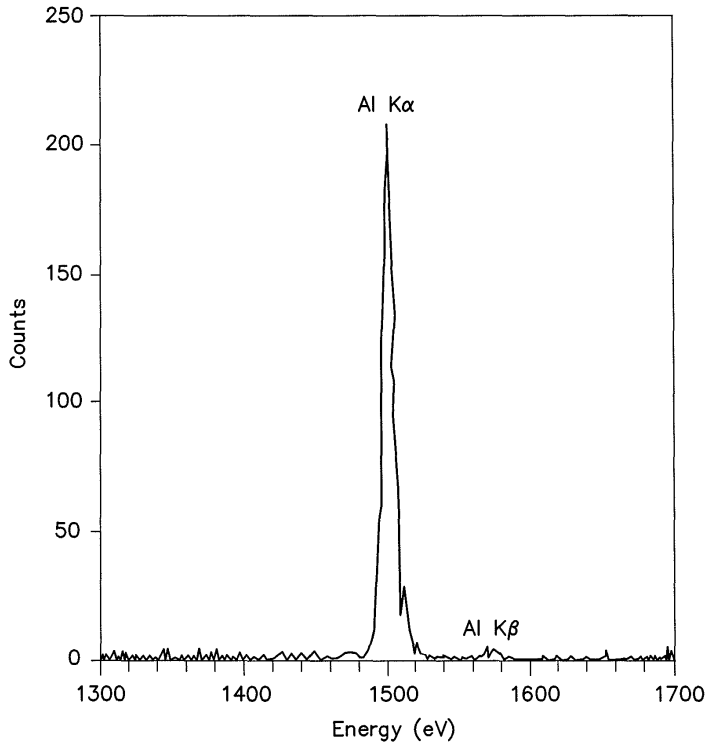
250
200
150
100
50
0
Counts
Al Kα
Al Kβ
1300
1400
1500
1600
1700
Energy (eV)

Concentric Hemispherical Analyzer (CHA)

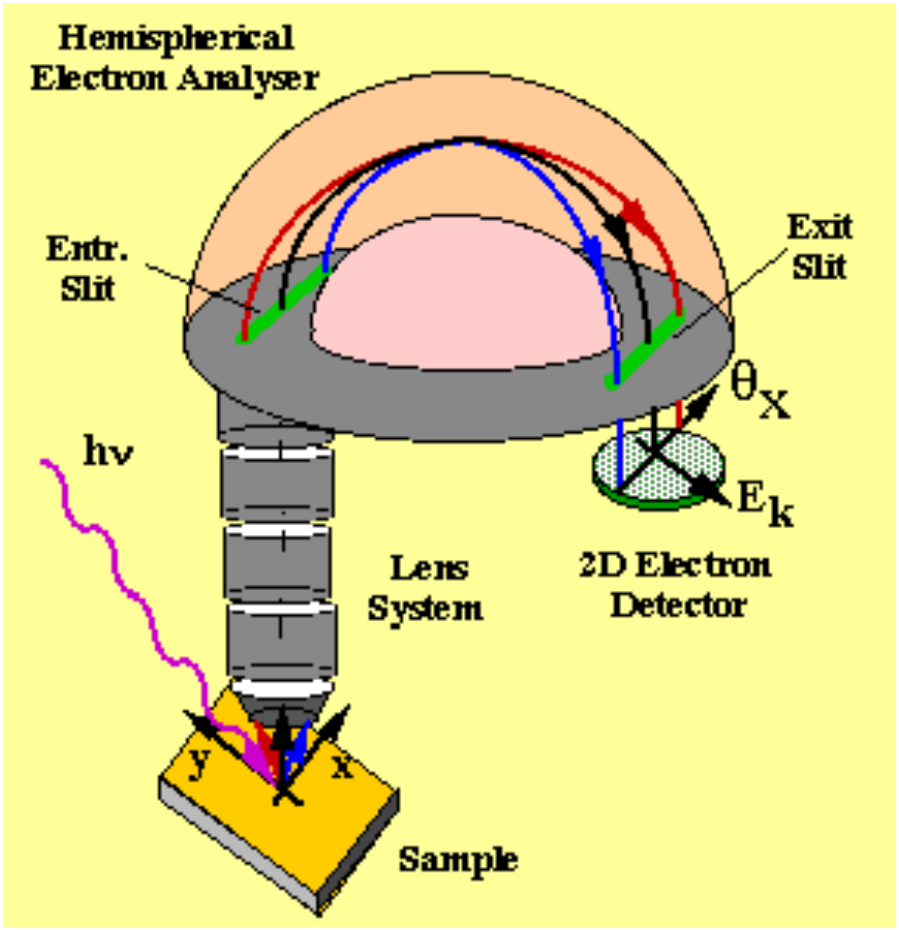

$\Delta E/E_0 = s/ R_0$

s: mean slit width; R_0: mean radius

Angle-resolved photoemission spectroscopy (ARPES)

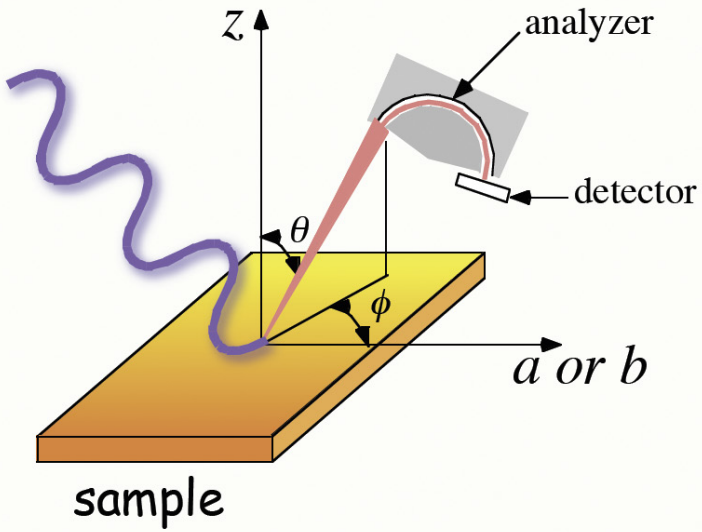

We need:

binding energy - E_b

initial momentum - k^i

$$E_b = E - h\nu + W$$

$$k^i_{||} = k^f_{||} = \sqrt{2mE/\hbar^2}\sin\theta$$

$$k^i_{\perp} = k^f_{\perp} - G = \sqrt{2mE/\hbar^2}\cos\theta - G$$

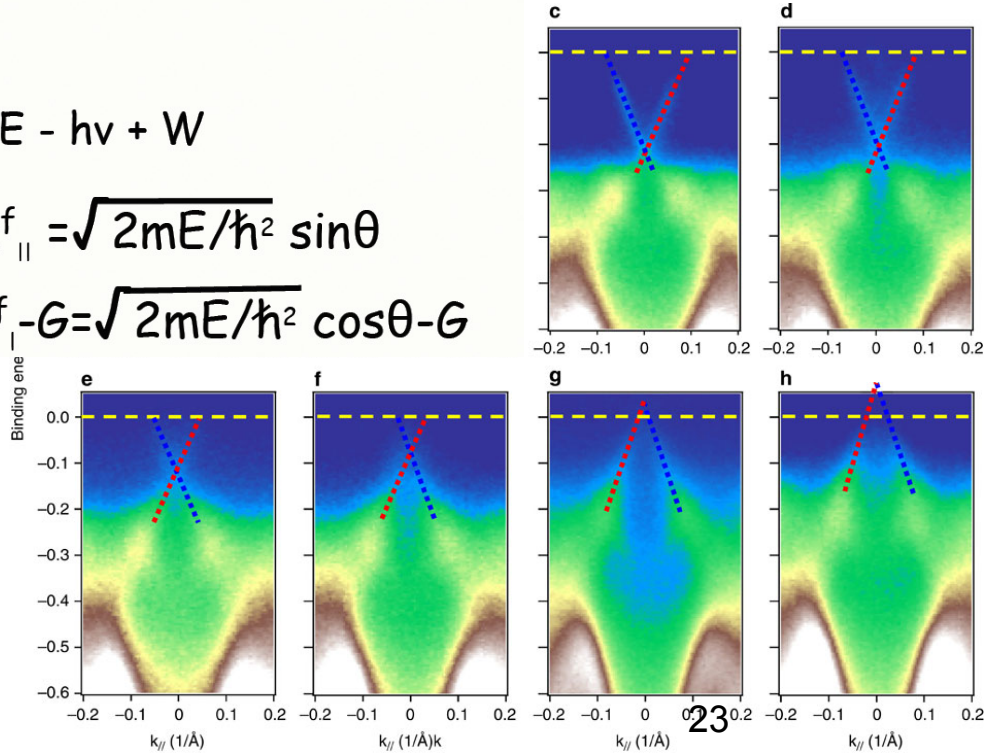

Spectroscopy at nanometer scale

1. Spectroscopy vs. Microscopy
2. Spectroscopies for H and H_2
3. Physics and Chemistry of nanomaterials

Microscopy is the science of investigating small objects that are too small for the naked eye. The microscopic study involves revelation of the structure and morphology of the matter under investigation.

Spectroscopy is the study of the interaction between matter and radiated energy. With the mechanism of "resonance", the characteristic nature of the matter can be probed.

Both microscopic and spectroscopic techniques are essential for nanoscience research.

Spectroscopy originates from the dispersion of light through a prism.

Prism

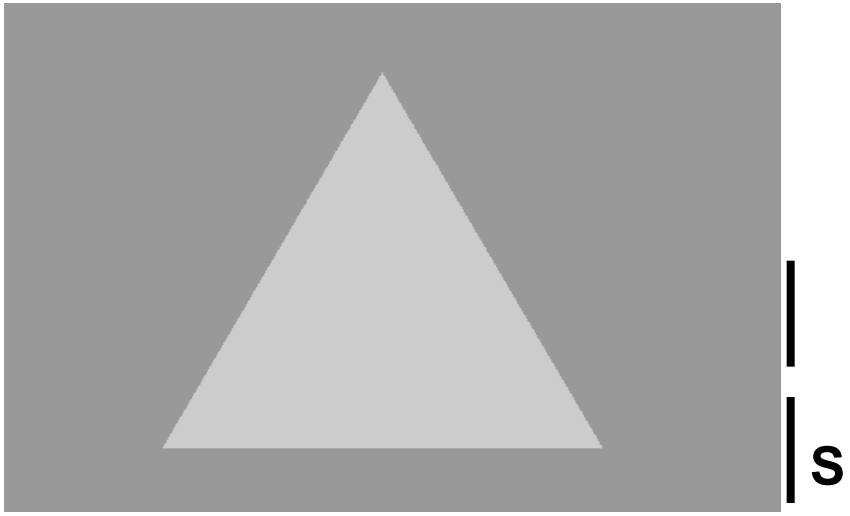

Grating

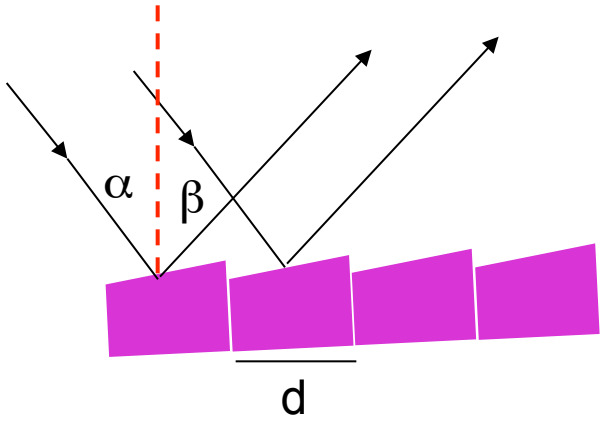

$\Delta s = d\,(\sin\alpha - \sin\beta)$
$= m\lambda$

Mechanical resonance

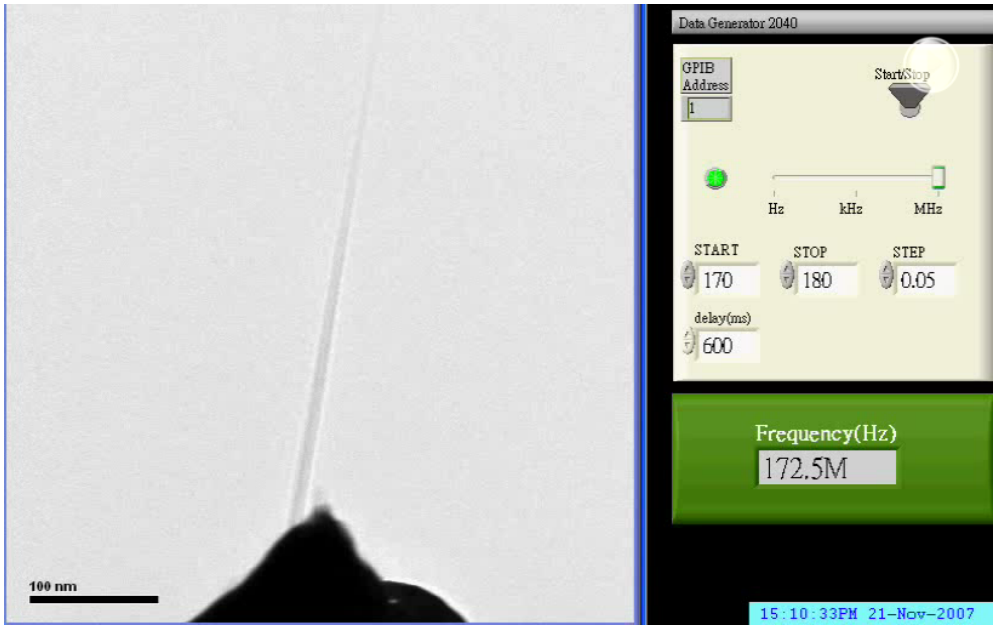

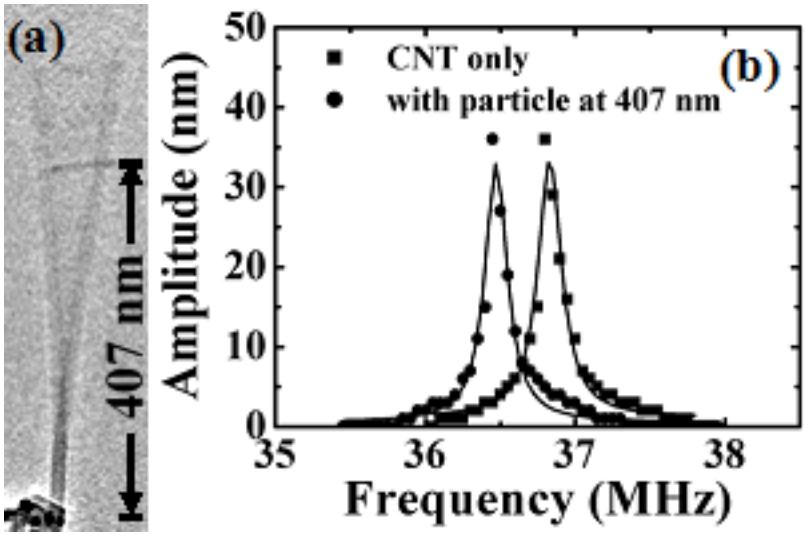

Bohr model of hydrogen atom

$$E = -\frac{Z^2 me^4}{8n^2h^2\varepsilon_0^2} = \frac{-13.6Z^2}{n^2}eV \qquad r = \frac{n^2h^2\varepsilon_0}{Z\pi me^2} = \frac{n^2a_0}{Z}$$

$$a_0 = 0.0529nm = Bohr\ radius$$

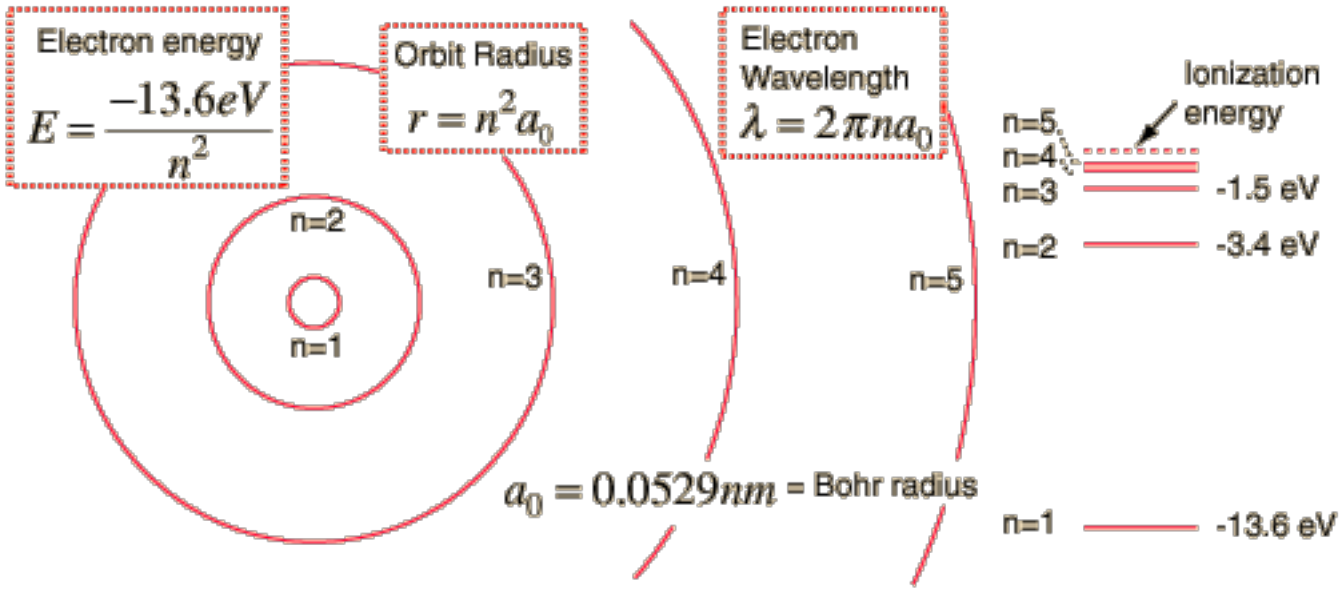

Electron Transitions

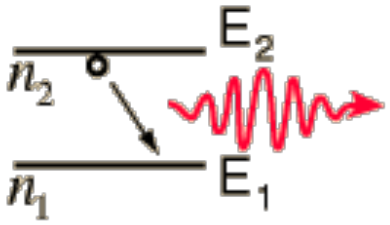

A downward transition involves emission of a photon of energy:

$$E_{photon} = h\upsilon = E_2 - E_1$$

Given the expression for the energies of the hydrogen electron states:

$$h\upsilon = \frac{2\pi^2 me^4}{h^2}\left[\frac{1}{n_1^2} - \frac{1}{n_2^2}\right] = -13.6\left[\frac{1}{n_1^2} - \frac{1}{n_2^2}\right] \text{eV}$$

Fermi's golden rule is a way to calculate the transition rate (probability of transition per unit time) between two eigenstates

$$T_{i\to f} = \frac{2\pi}{\hbar}\left|\langle f|H'|i\rangle\right|^2 \rho,$$

Absorption spectra of atomic hydrogen

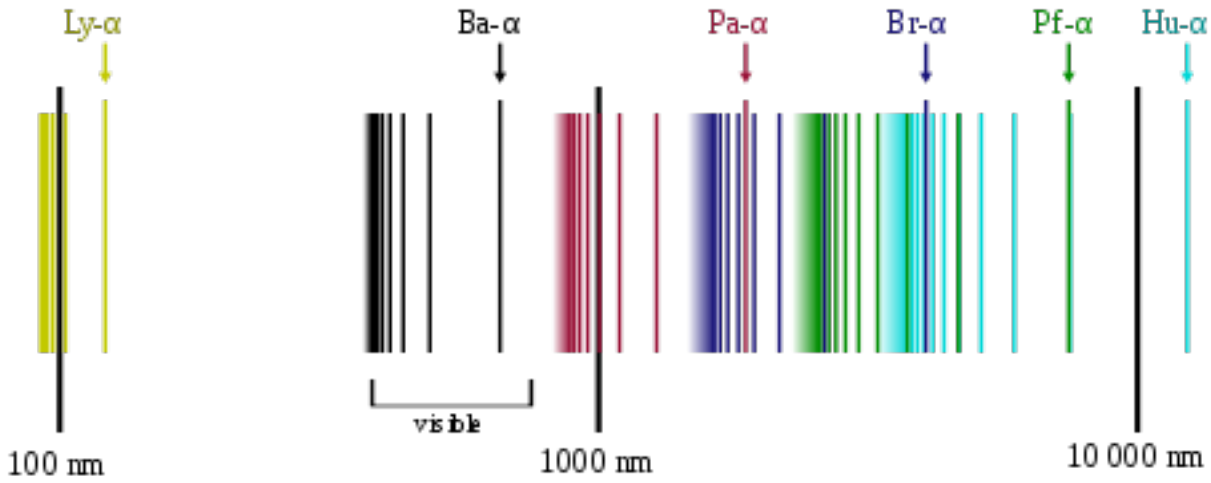

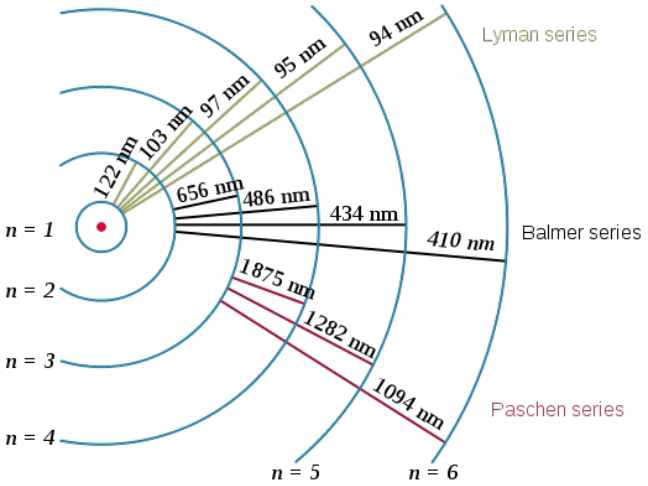

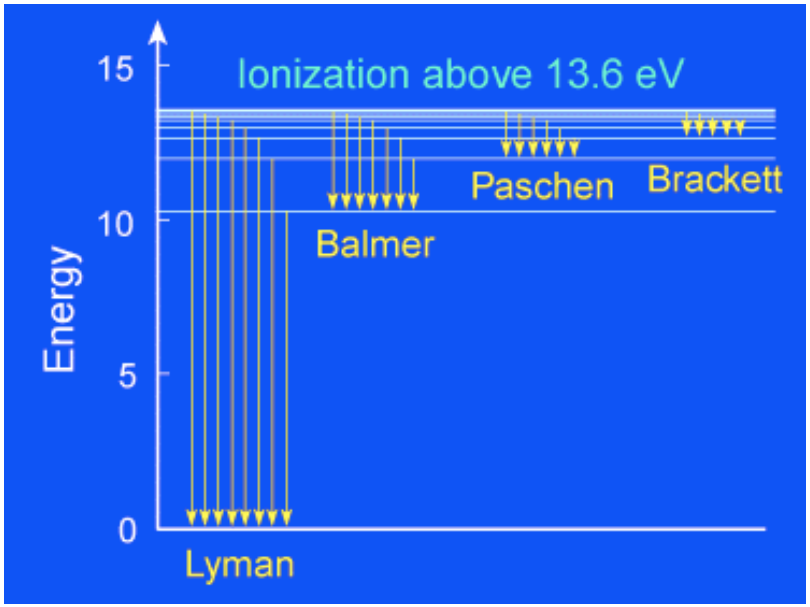

Absorption spectra of molecular hydrogen

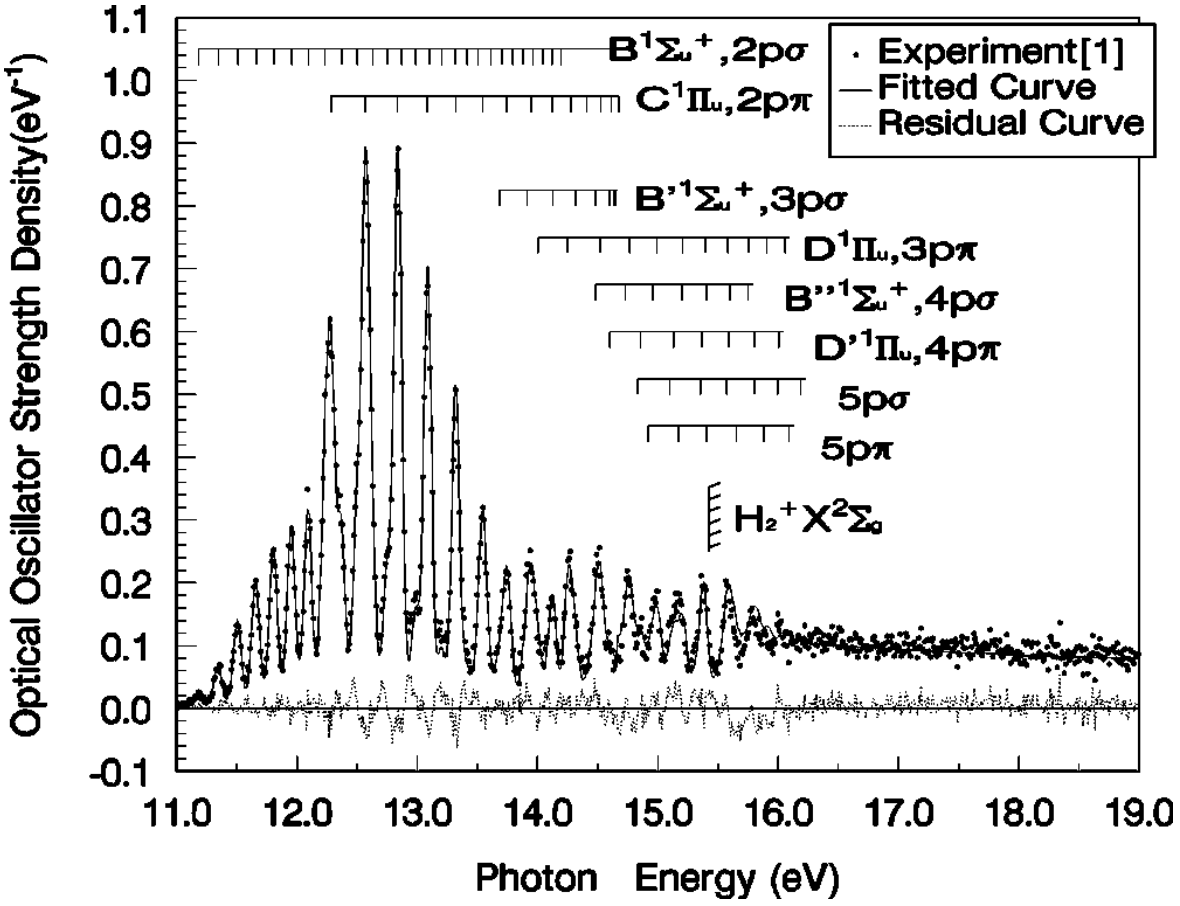

Zhi Ping Zhong et al., Phys. Rev. A **60**, 236 (1999)

One dimensional size effect

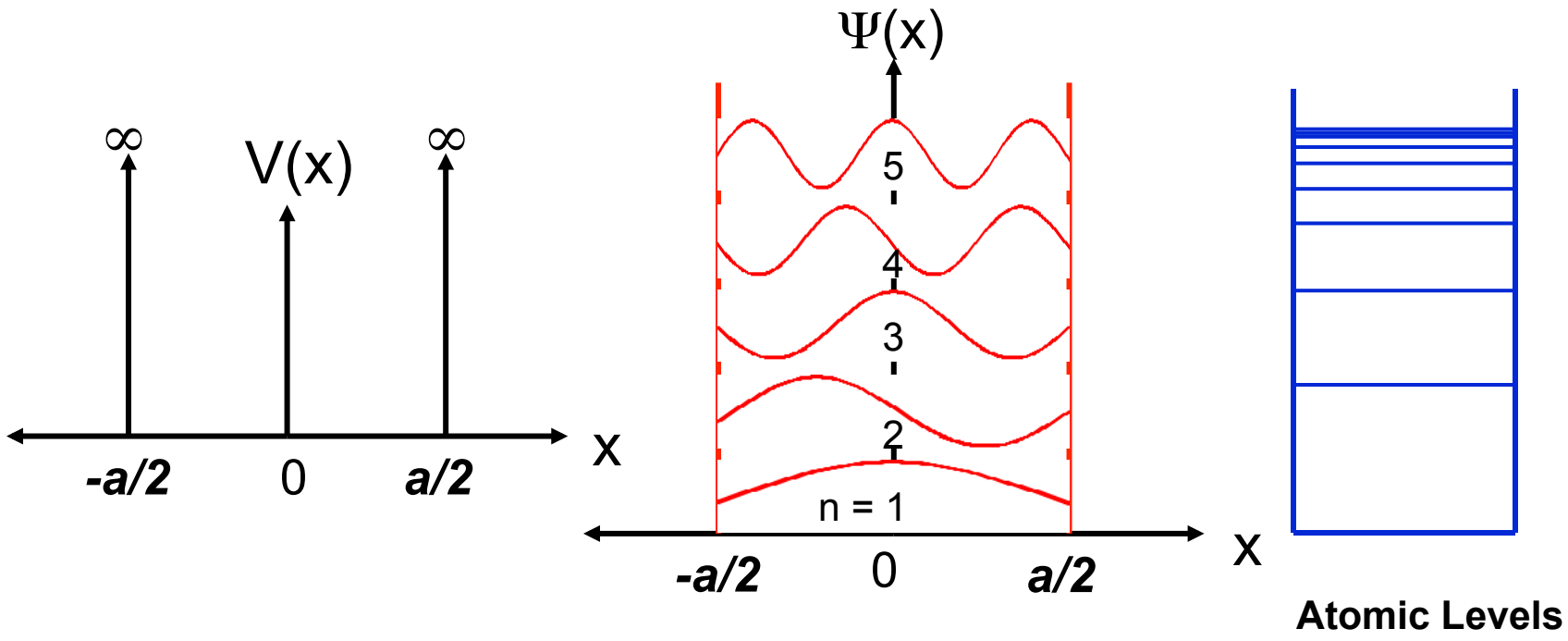

$$\Psi(x) = \begin{cases} \sin(n\pi x/a), & n \text{ even} \\ \cos(n\pi x/a), & n \text{ odd} \end{cases}$$

$$E = n^2\pi^2\hbar^2/2ma^2,\ n = 1,2,3\ldots$$

Size effect

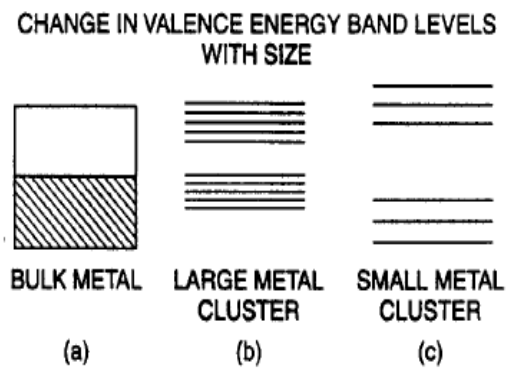
CHANGE IN VALENCE ENERGY BAND LEVELS WITH SIZE
BULK METAL
LARGE METAL CLUSTER
SMALL METAL CLUSTER
(a)
(b)
(c)

Size

Au nanoparticle as an example

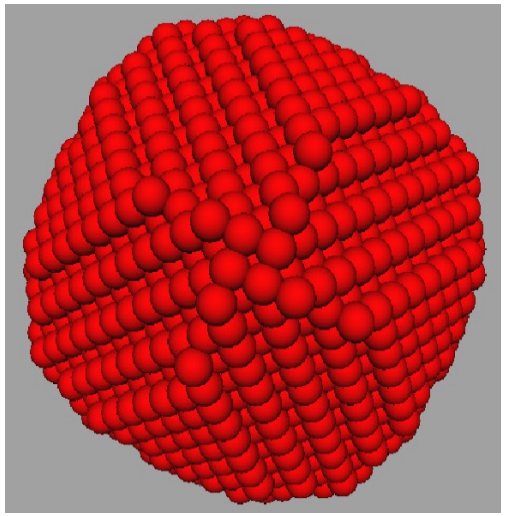

$$E_F = (\hbar^2/2m)\,(3\pi^2 n)^{2/3}$$

$$g(E_F) = (3/2)\,(n/E_F)$$

$$\delta = 2/[g(E_F)V] = (4/3)\,(E_F/N)$$

Number of valence electrons (N) contained in the particles is roughly 40,000. Assume the Fermi energy (E_F) is about 7 eV for Au, then

$$\delta \sim 0.22 \text{ meV} \sim 2.5 \text{ K}$$

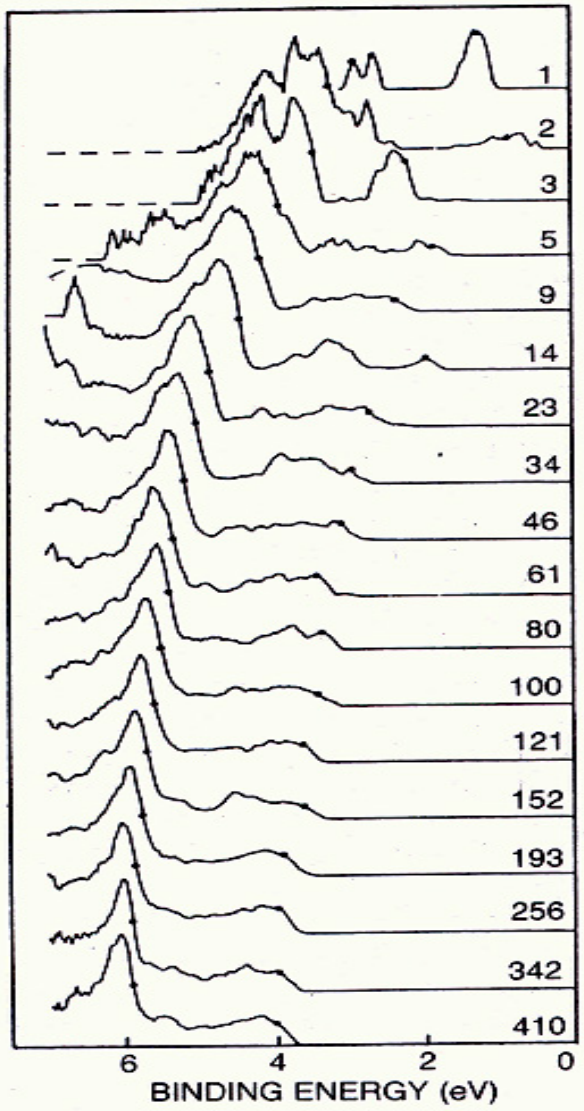

Ultraviolet photoemission spectra of ionized copper clusters Cu_N^- ranging in size from N of 1 to 410 show the energy distribution versus binding energy of photoemitted electrons. These photoemission patterns show the evolution of the 3d band of Cu as a function of cluster size. As the cluster size increases, the electron affinity approaches the value of the bulk metal work function. (Adapted from ref. 10.) **Figure 5**

Semiconductor quantum dots

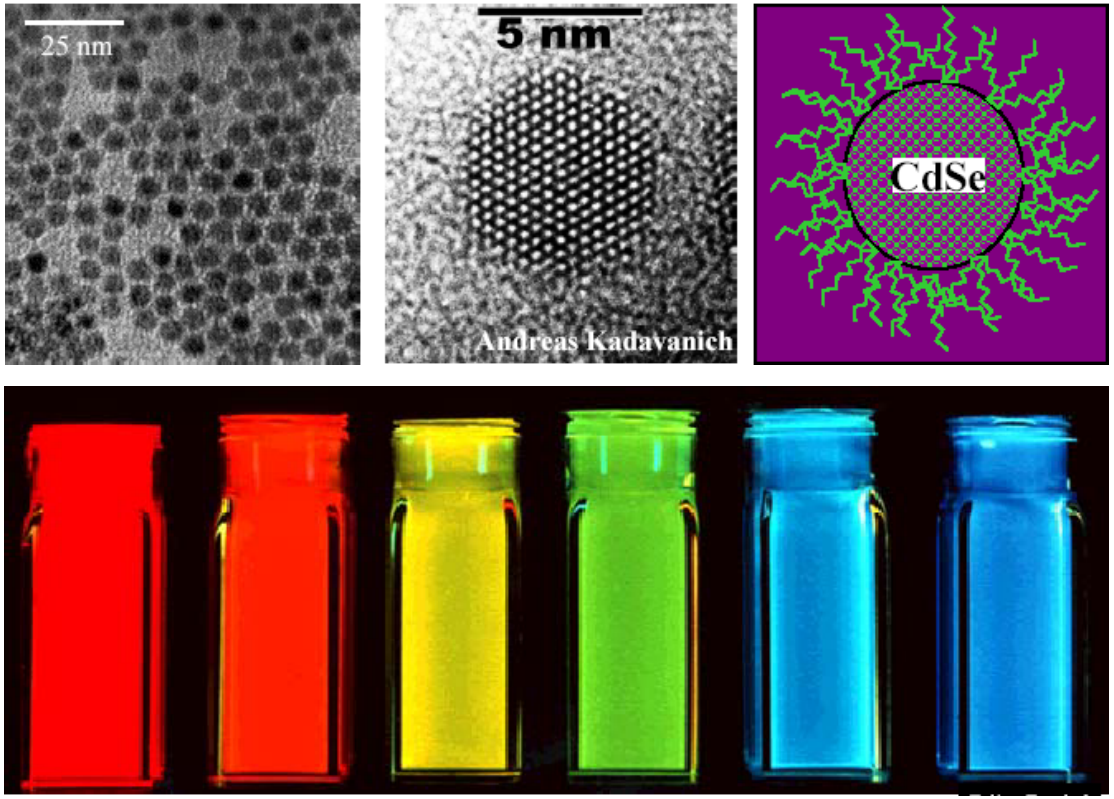

(Reproduced from Quantum Dot Co.)

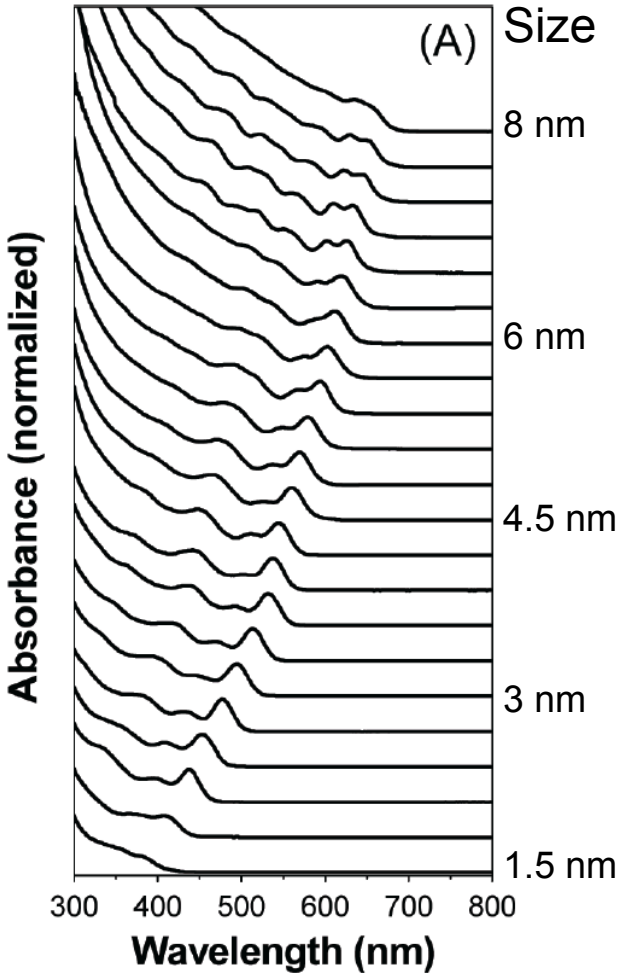

Ratio of surface atoms

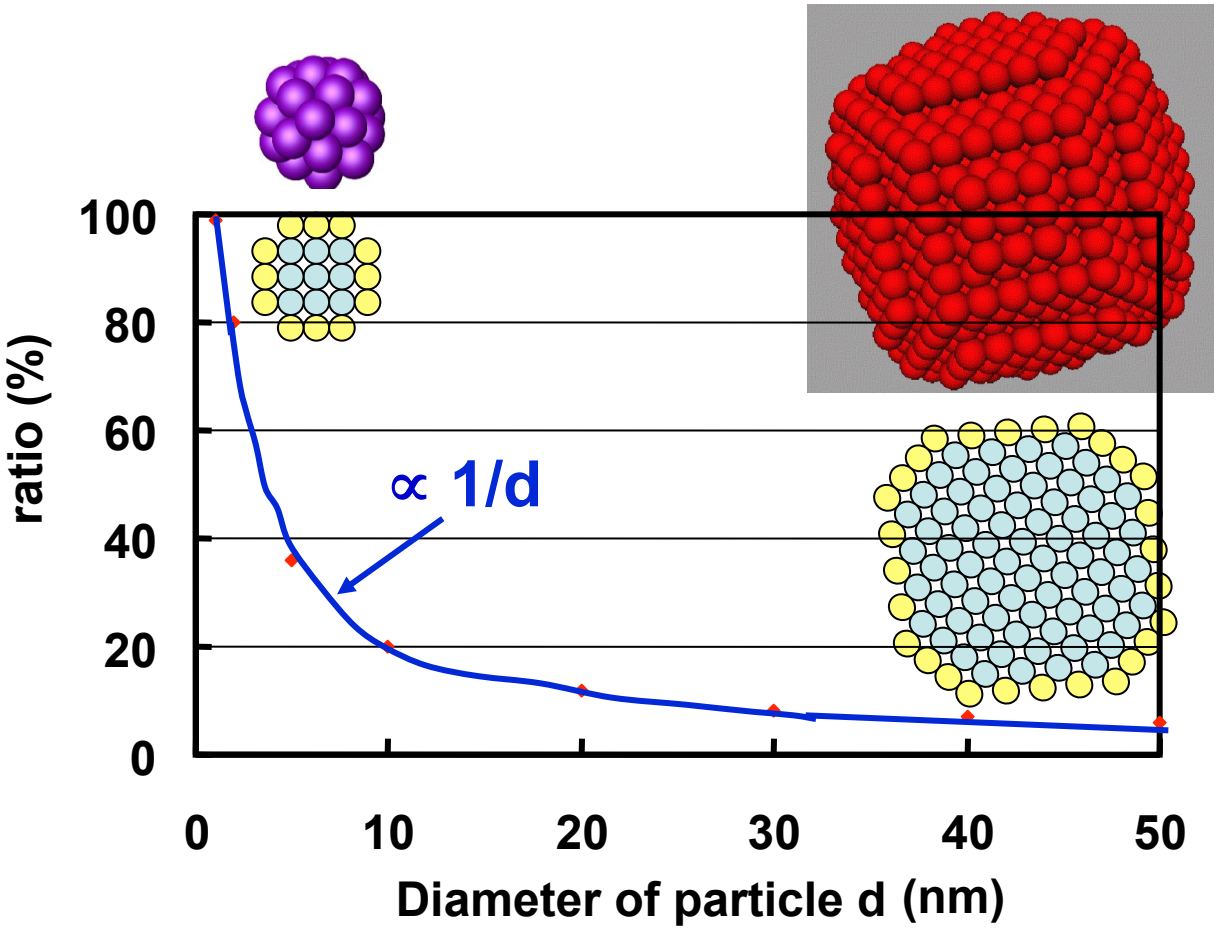

Optical properties of nanoparticles (in the infrared range)

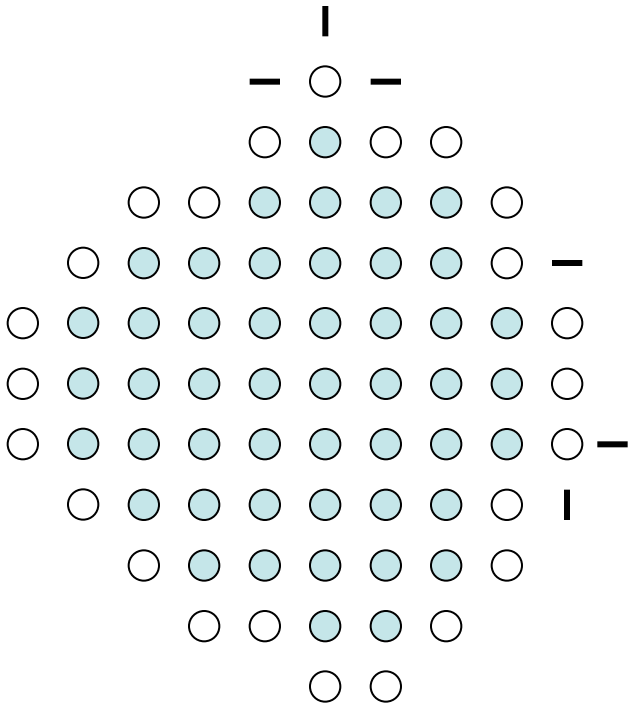

(1) Broad-band absorption:
Due mainly to the increased normal modes at the surface.

(2) Blue shift:
Due mainly to the bond shortening resulted from surface tension or phonon confinement.

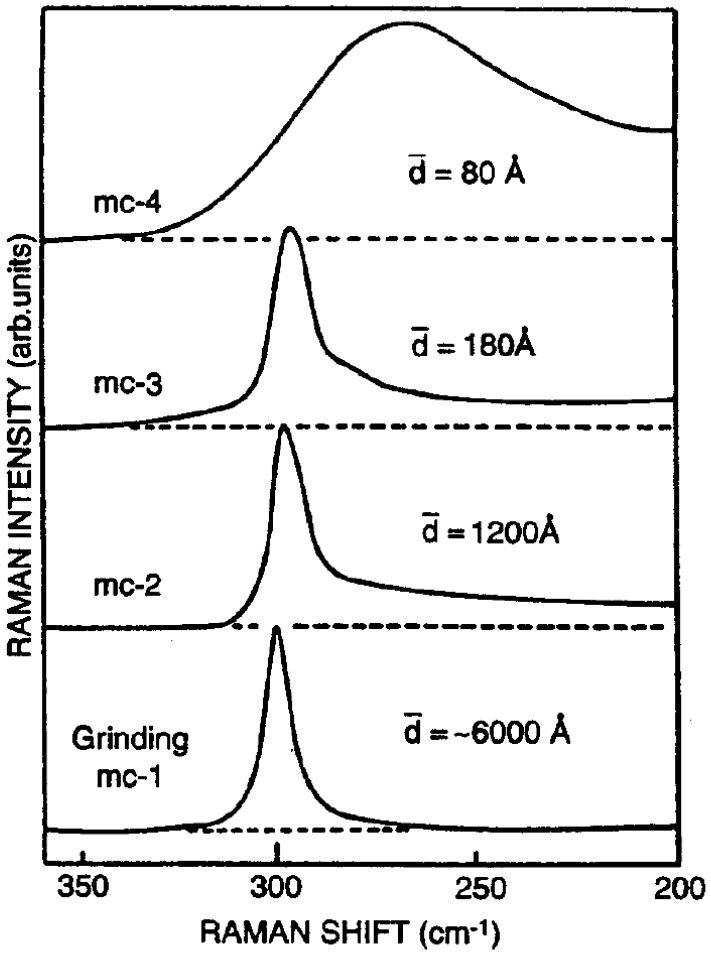

Figure 8.11. Raman spectra of Ge nanocrystallites produced by gas condensation showing the broadening and shift to lower wavenumbers as the particle size decreases. The lowest spectrum was obtained from ground bulk germanium. [From S. Hayashi, M. Ito, and H. Kanamori, *Solid State Commun.* **44**, 75 (1982).]

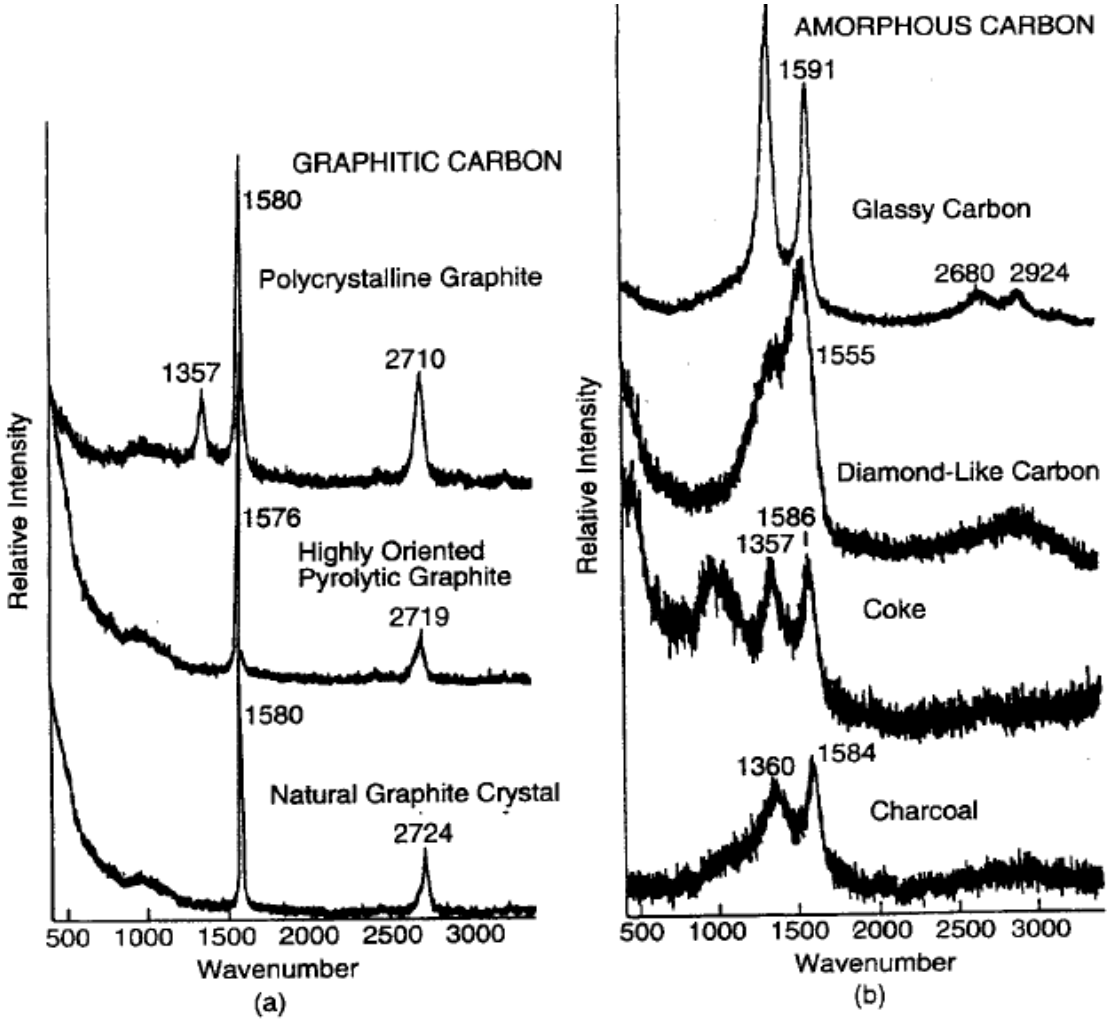

Figure 8.19. Raman spectra of (a) crystalline graphites and (b) noncrystalline, mainly graphitic, carbons. The *D* band appears near 1355 cm^{-1} and the *G* band, near 1580 cm^{-1}. [From D. S. Knight and W. B. White, *J. Mater, Sci.* **4**, 385 (1989).]

Optical properties of nanoparticles (in the visible light range)

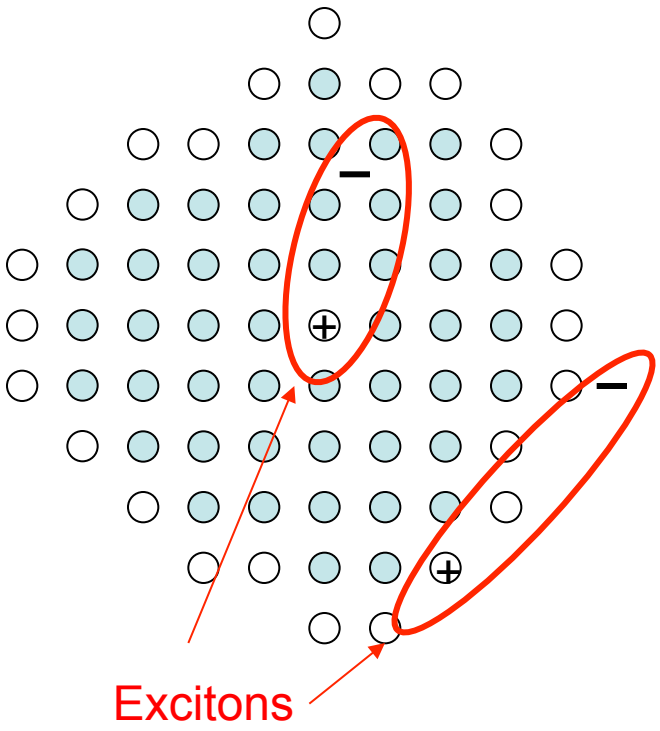

(1) Blue shift:
Due mainly to the energy-gap widening because of the size effect.

(2) Red shift:
Bond shortening resulted from surface tension causes more overlap between neighboring electron wavefunctions. Valence bands will be broadened and the gap becomes narrower.

(3) Enhanced exciton absorption:
Due mainly to the increased probability of exciton formation because of the confining effect.

Scanning Tunneling Spectroscopy

1. Barrier Height Imaging

Up to now homogeneous surfaces were considered. If there is an inhomogeneous compound in the surface the work function will be inhomogeneous as well. This alters the local barrier height. Differentiation of tunneling current yields

$$\frac{d(\ln I)}{ds} \propto \sqrt{\Phi}$$

Thus the work function can directly be measured by varying the tip-sample distance, which can be done by modulating the current with the feedback turned on.

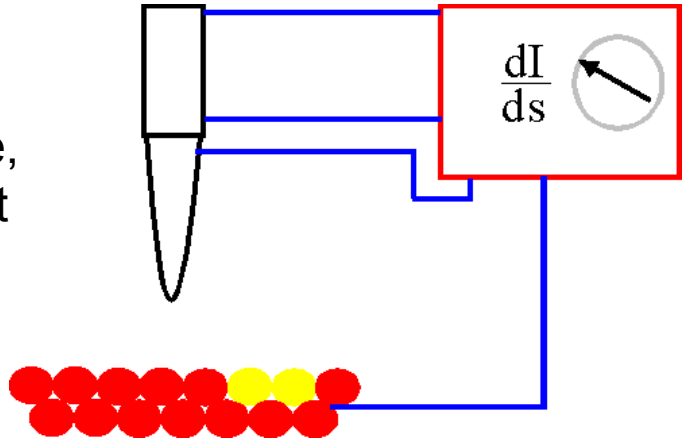

STM Images of Si(111)-(7×7)

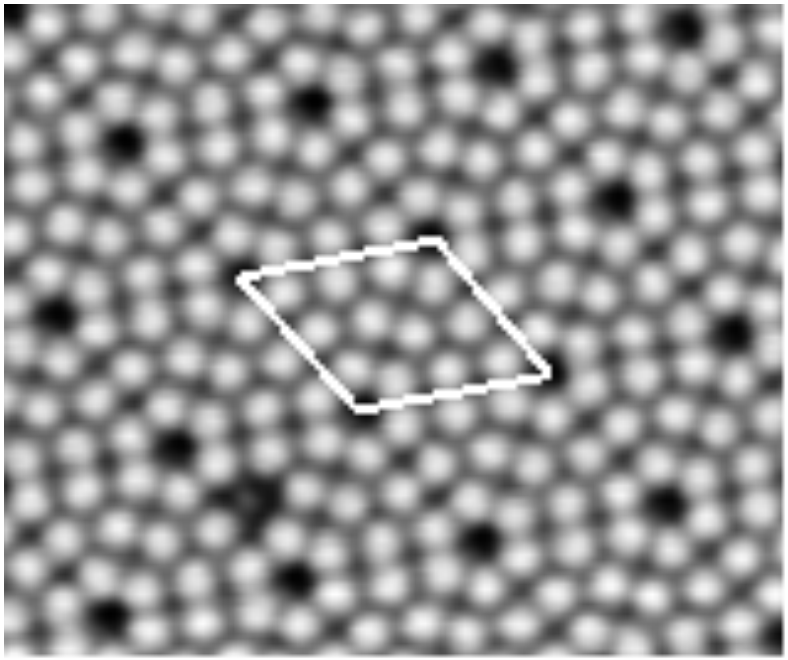

Empty-state image

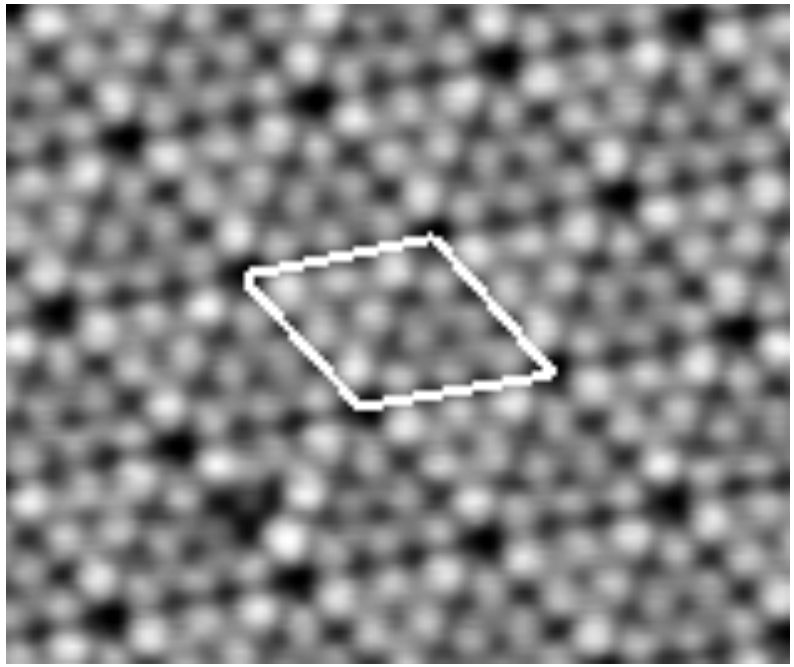

Filled-state image

Electronic Structures at Surfaces

Not Tunneling

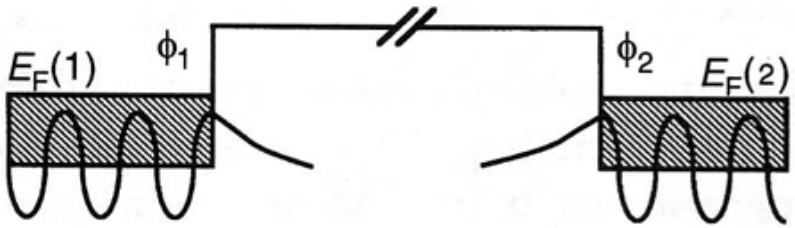

Empty-State Imaging

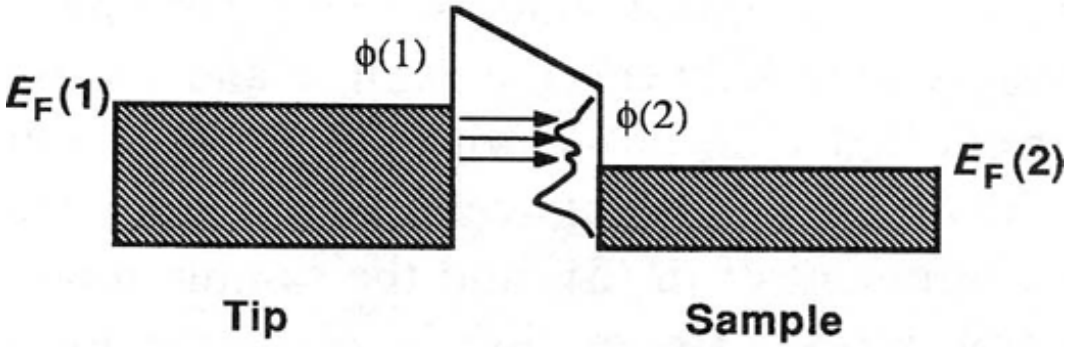

Tunneling

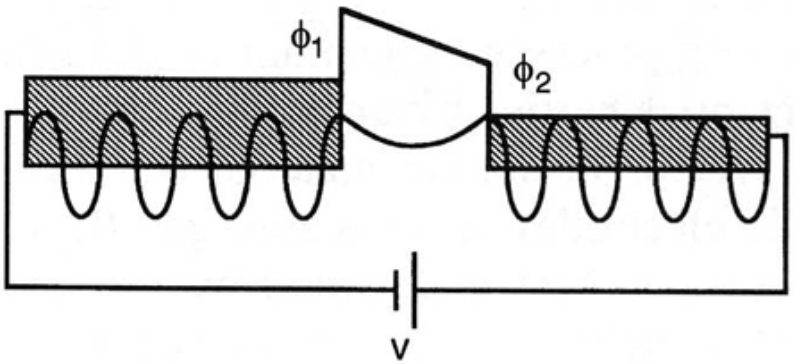

Filled-State Imaging

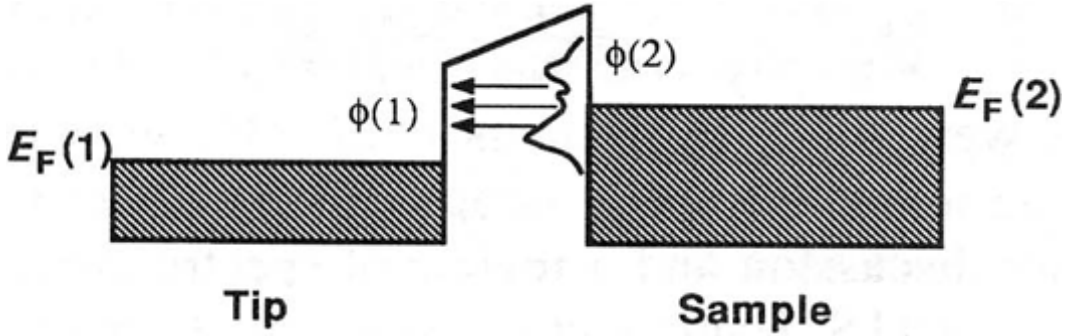

2. dI/dV imaging

If the matrix element and the density of states of the tip is nearly constant, the tunneling current can be estimated to

$$I \propto \int_0^{eV} \rho_{sa}\left(E_F - eV + \varepsilon\right) d\varepsilon$$

Differentiation yields the density of state

$$\frac{dI}{dV} \propto \rho_{sa}\left(E_F - eV\right)$$

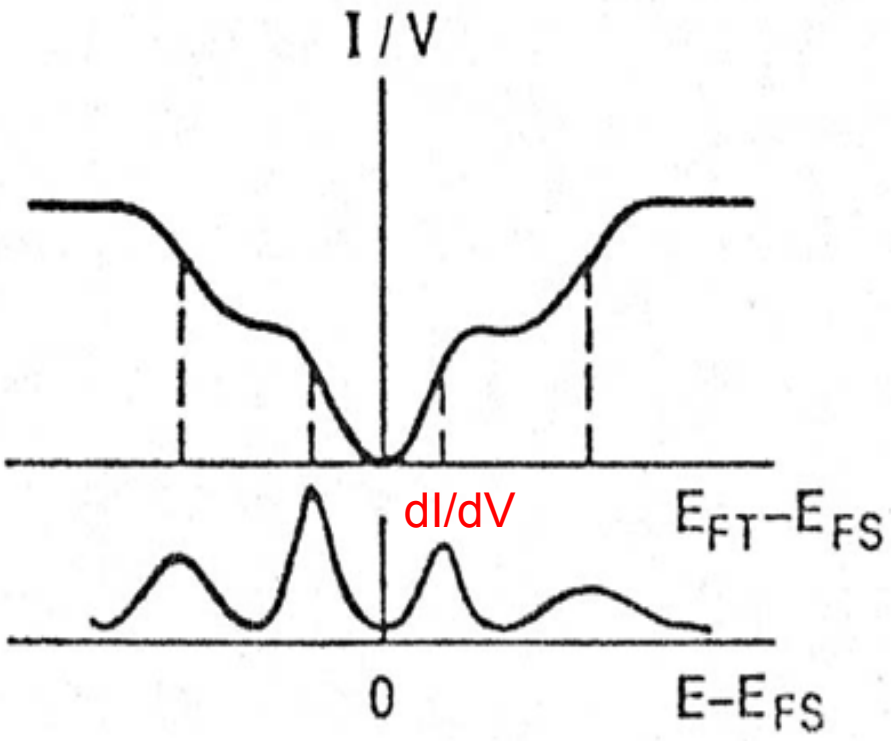

Density of state (DOS)

The mapping of surface density of states can be deduced by

- Modulation of the bias voltage (dI/dV imaging): The tip is scanned in the constant current mode to give a constant distance to the sample. A dither voltage of ~1k Hz is added to the bias voltage while the feedback loop remains active. A lock-in technique is employed to obtain the current change at the dither frequency.
- Current-Imaging Tunneling Spectroscopy (CITS): The tip is scanned in the constant current mode to give a constant distance to the sample. At each point the feedback loop is disabled and a current-voltage curve (I-V curve) is recorded.

STS of Si(111)-(7x7)

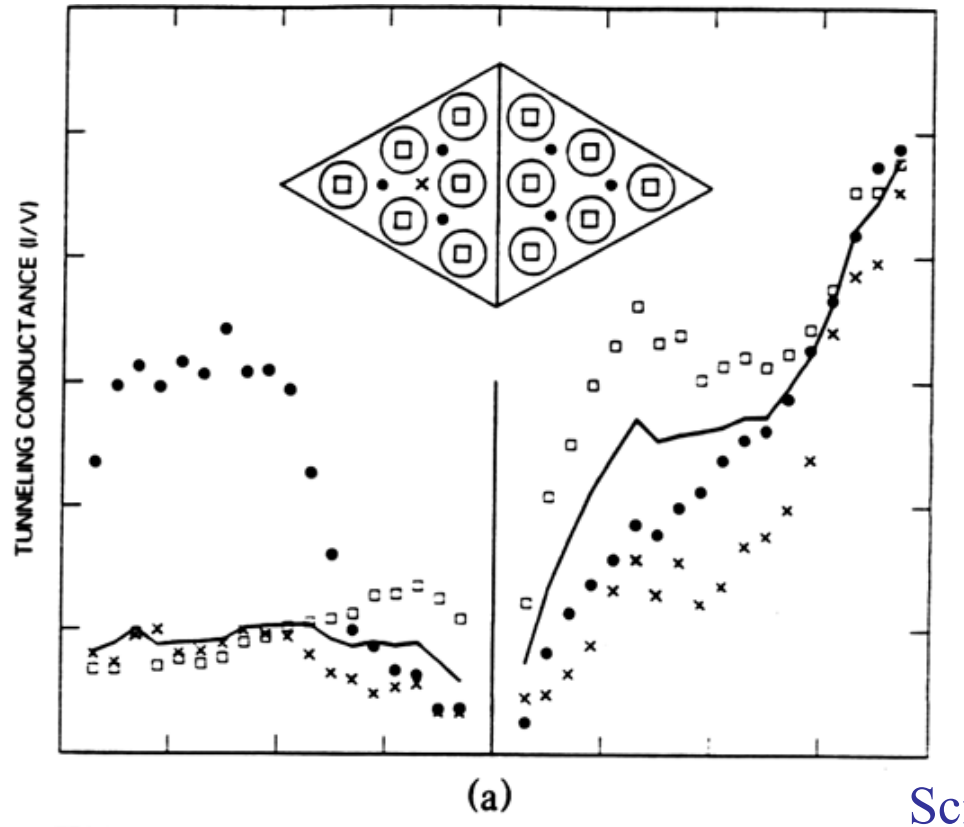

Science **234**, 304 (1986).

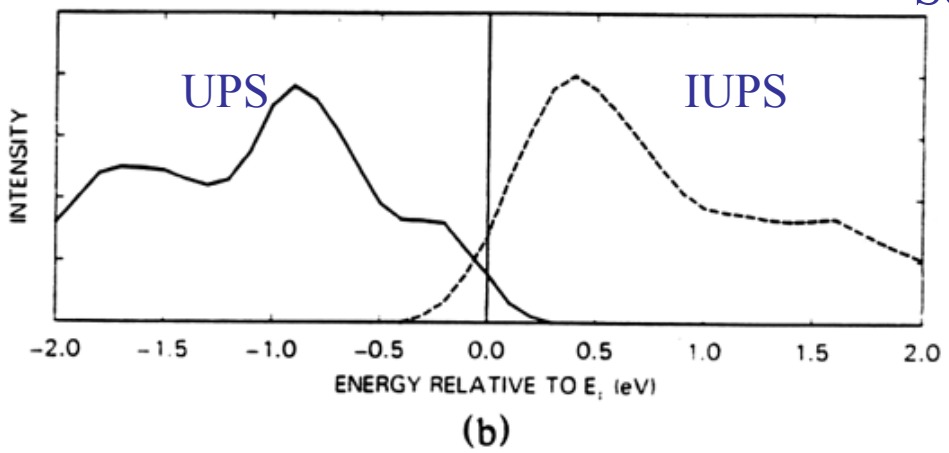

STS of Si(111)-(7x7)

topograph

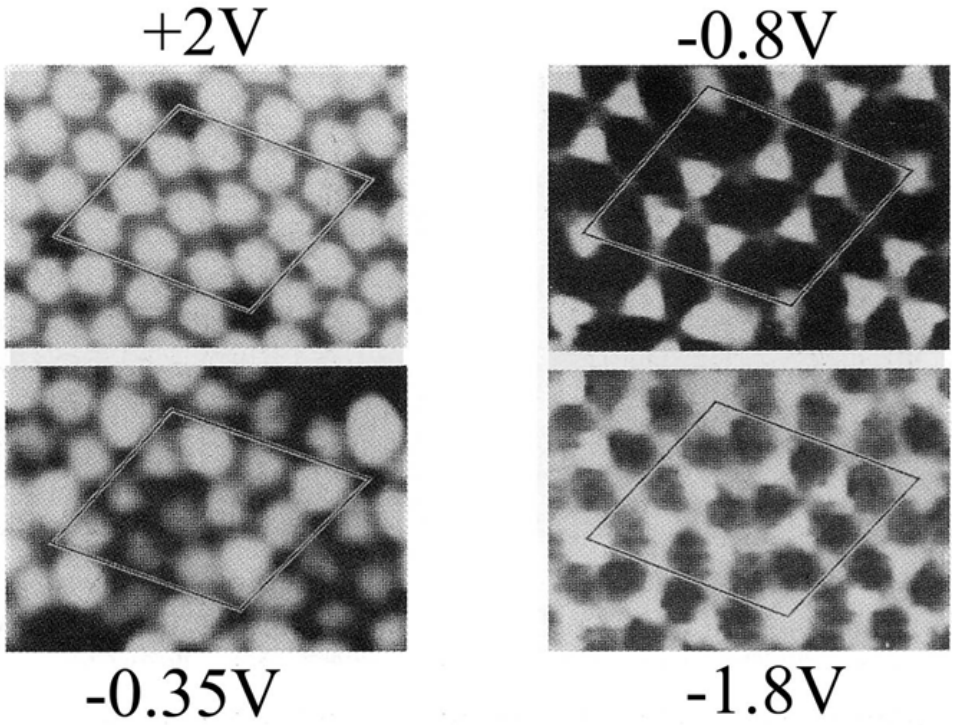

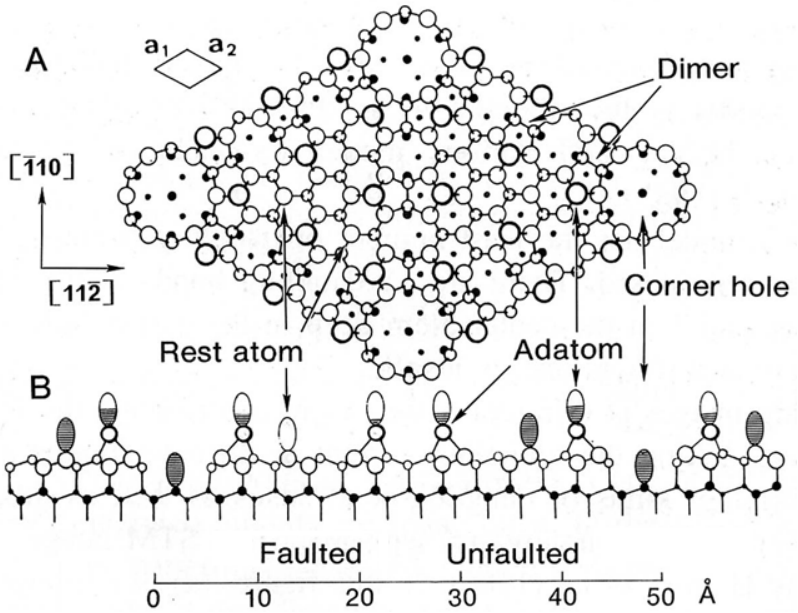

1. Science **234**, 304-309 (1986).
2. Phys. Rev. Lett. **56**, 1972-1975 (1986).

Density of states of various dimensions

3D

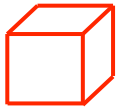

$D(\varepsilon) \sim \varepsilon^{1/2}$

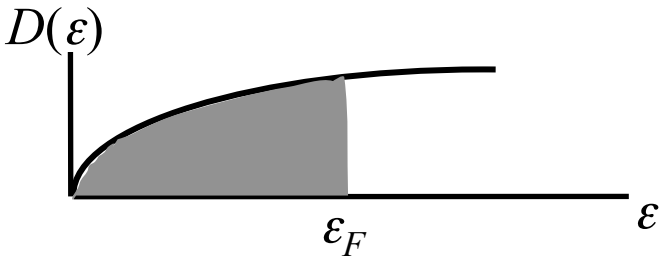

2D

$D(\varepsilon) = m^* / \pi\hbar^2$

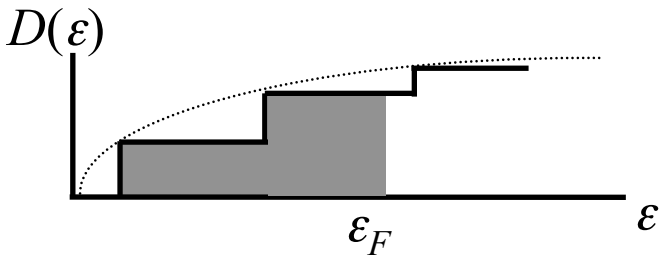

1D

$D(\varepsilon) \sim (\varepsilon - E_n)^{-1/2}$

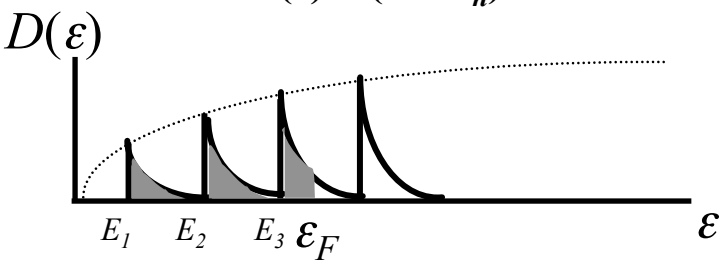

0D

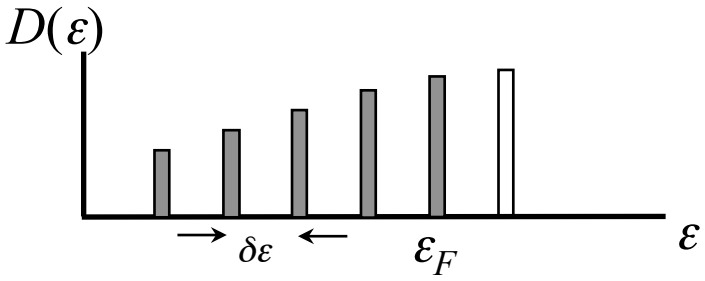

Electronic Structure of Single-wall Nanotubes

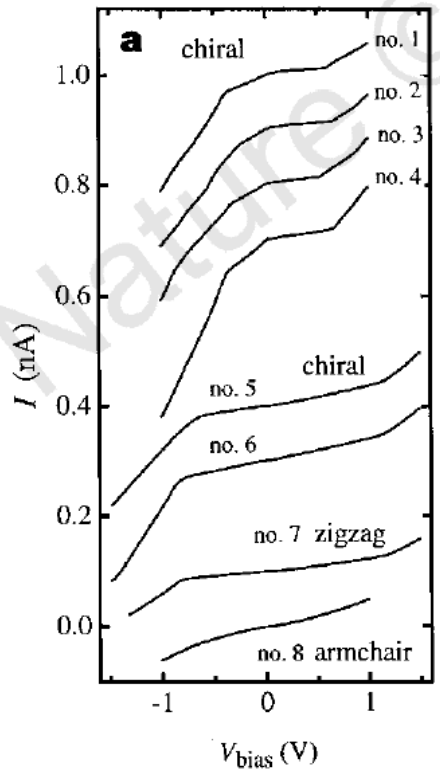

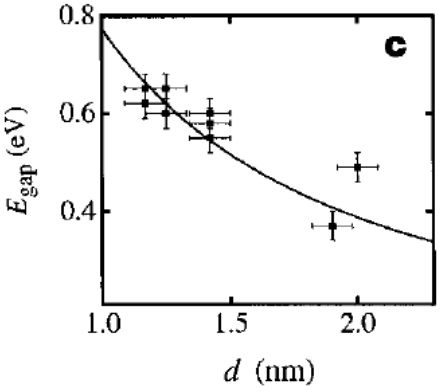

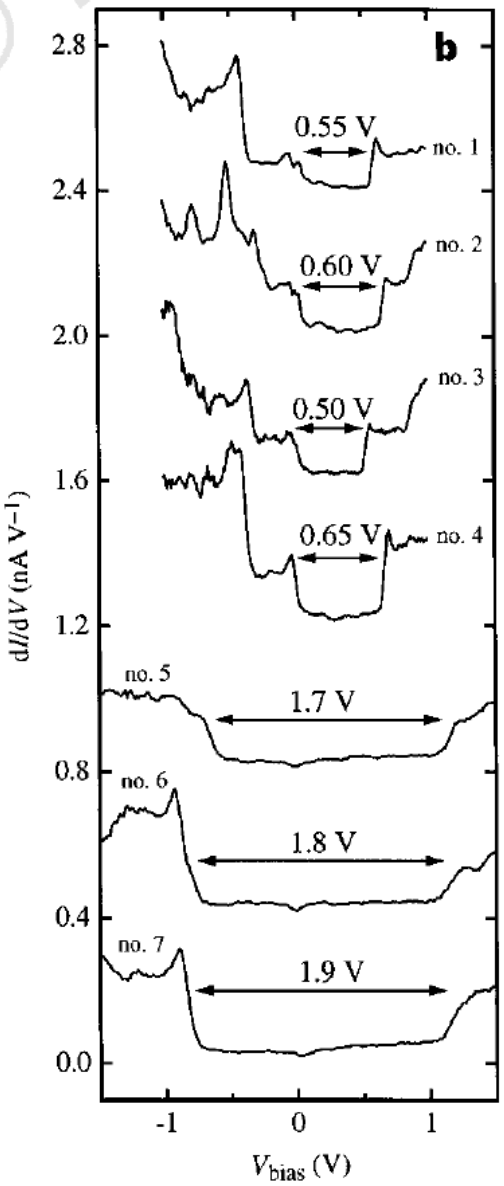

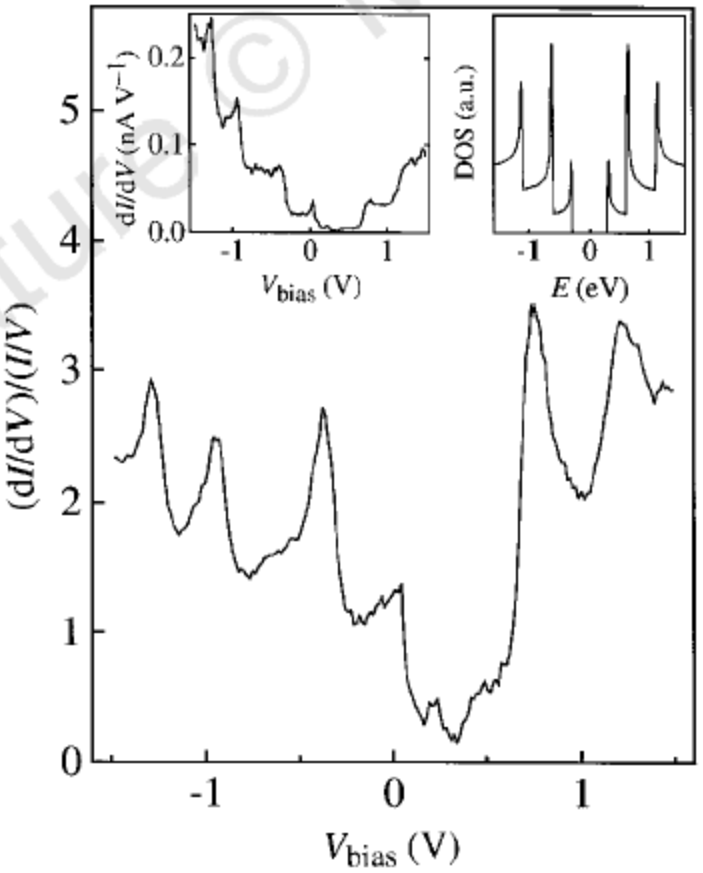

Nature **391**, 59 (1998).

Quantum size effect

λ = de Broglie wavelength of electron
a = thickness of metal film

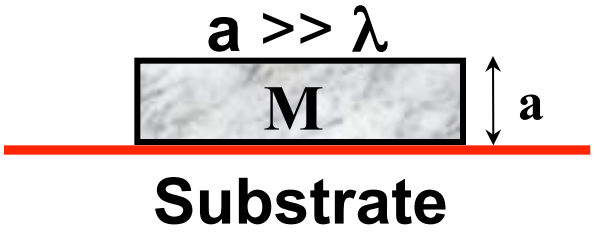

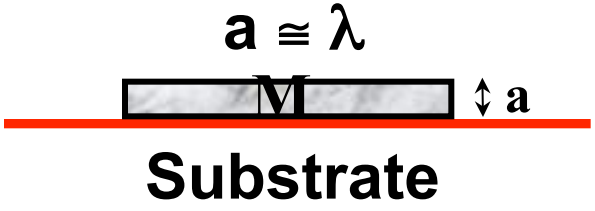

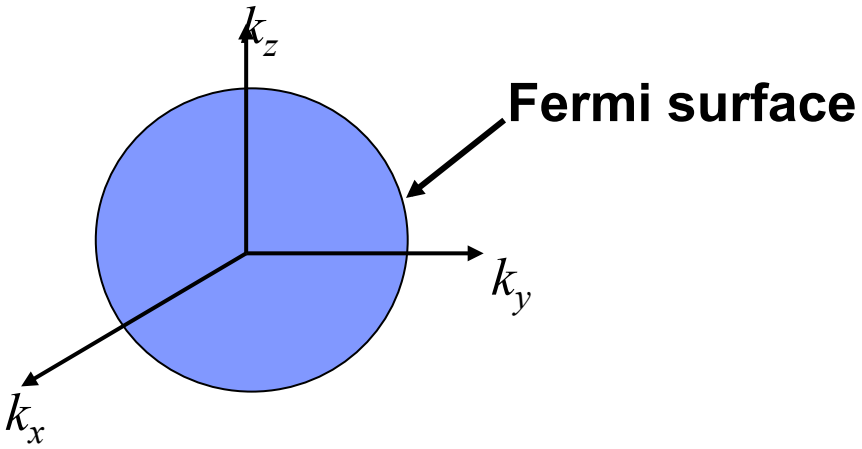

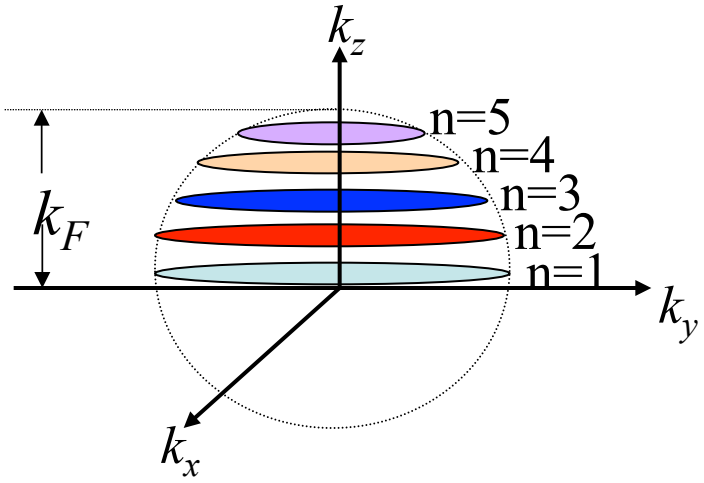

Pb islands on the IC Pb/Si(111)

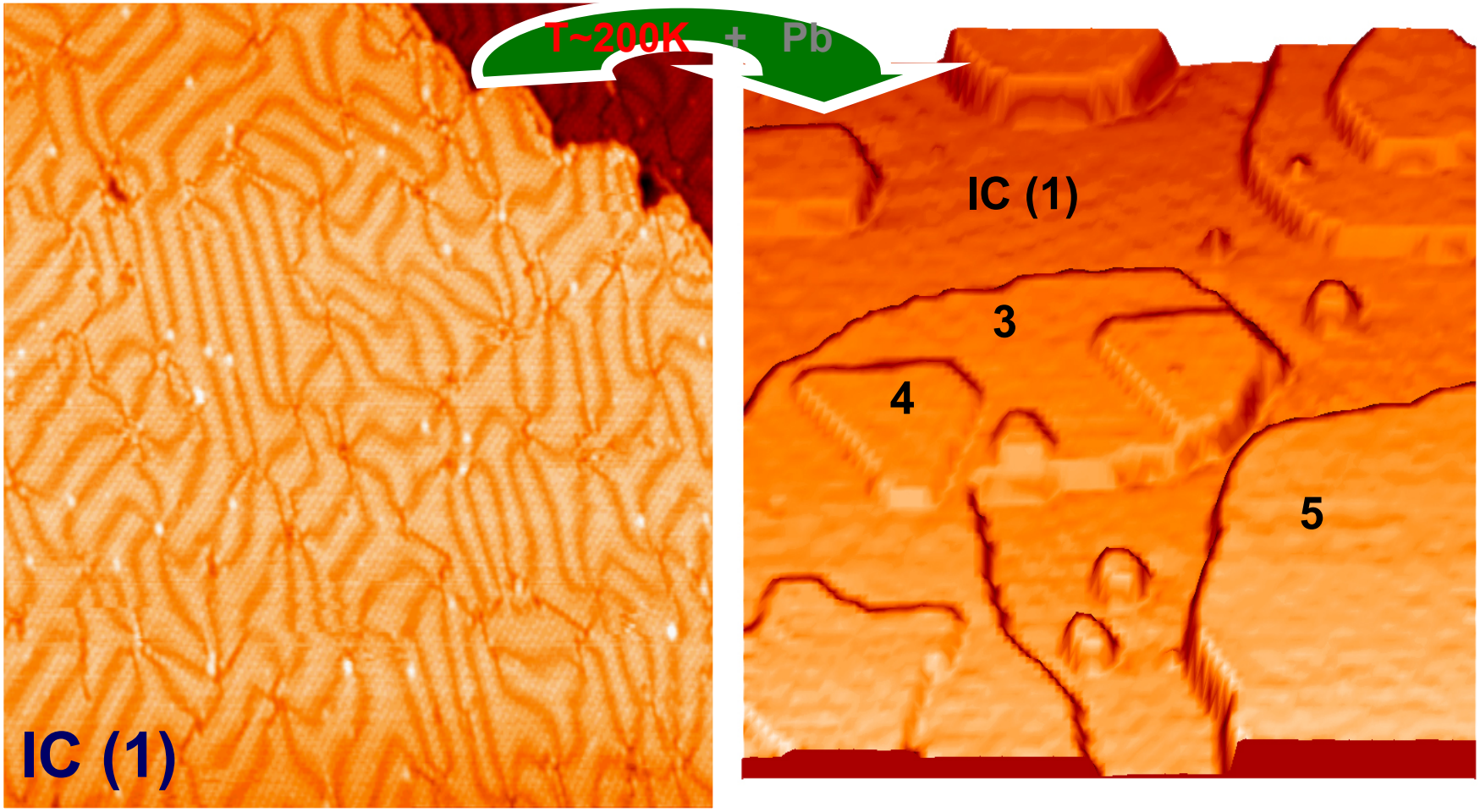

Spectra for Pb Films

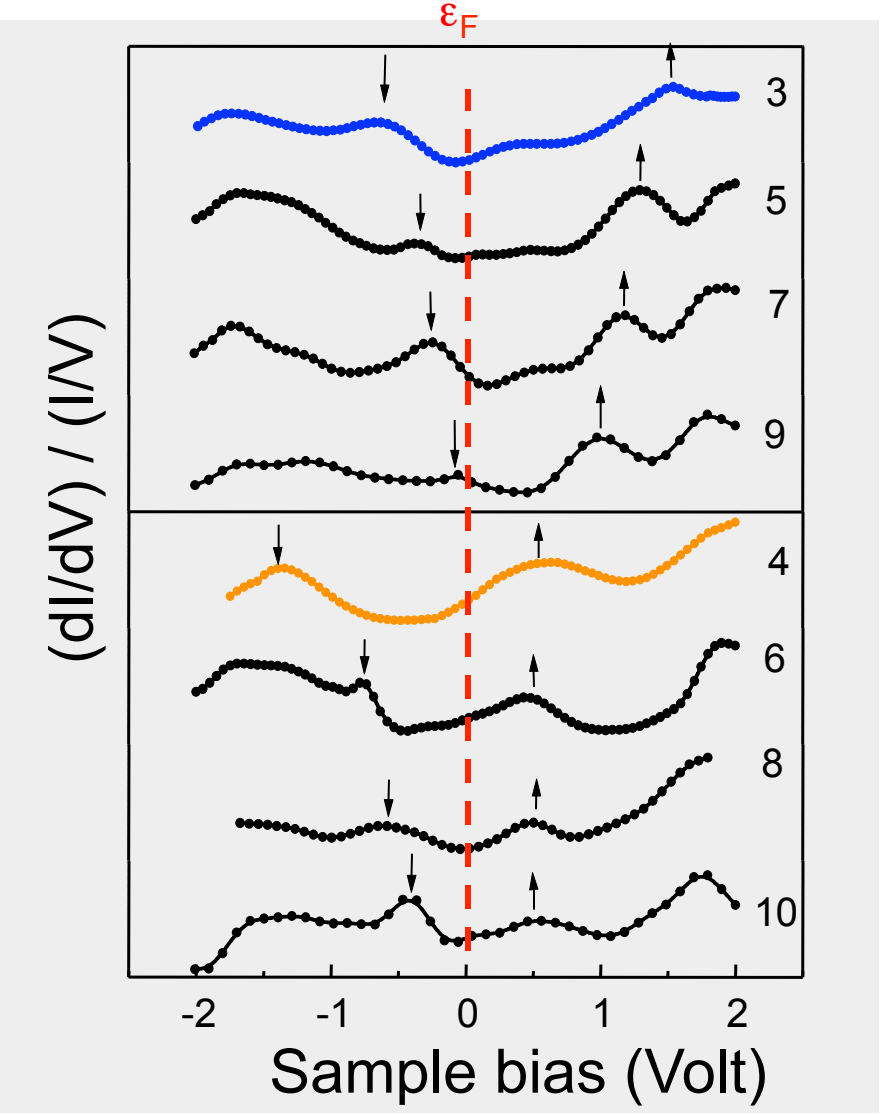

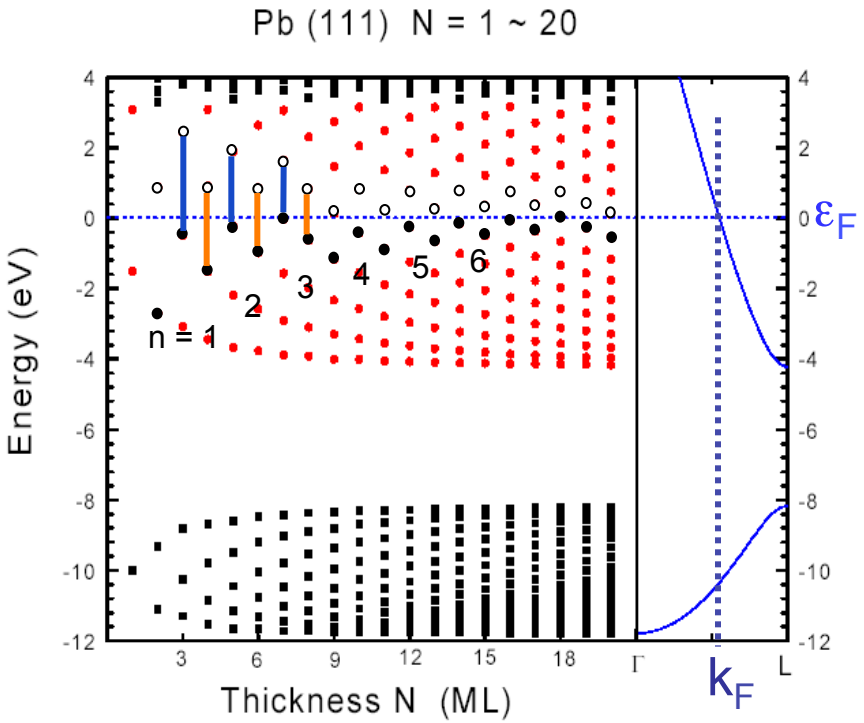

C.M. Wei and M.Y. Chou

$d_0 = 2.85$ Å $\lambda_F = 3.94$ Å

$2d_0 \approx 3(\lambda_F/2)$

Inelastic Tunneling

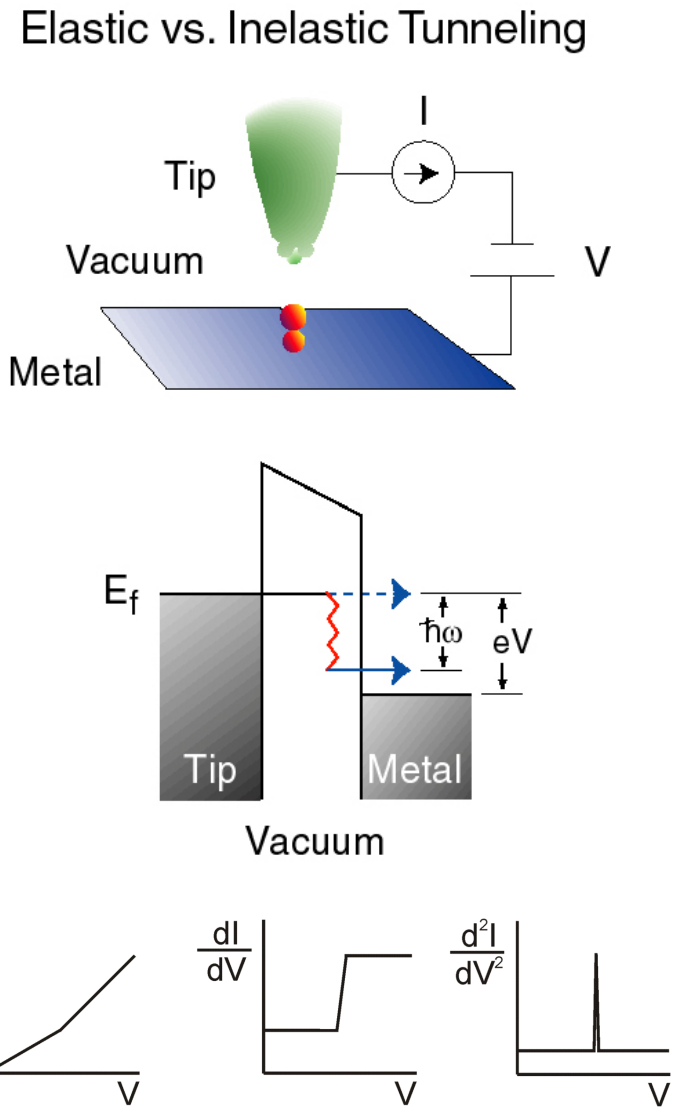

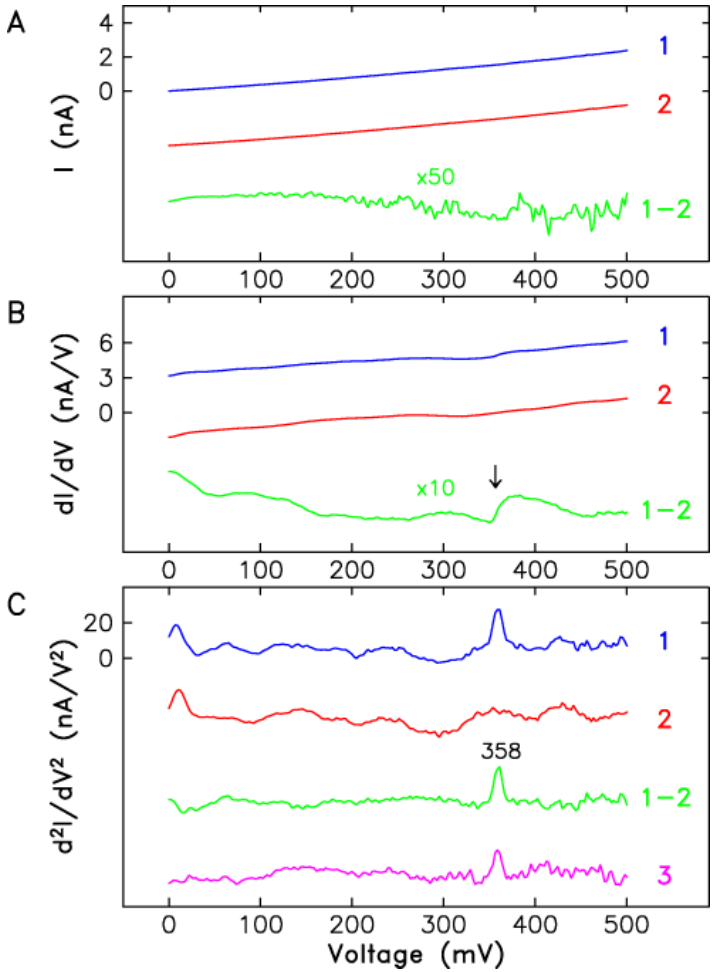

Single Molecule Vibrational Spectroscopy and Microscopy

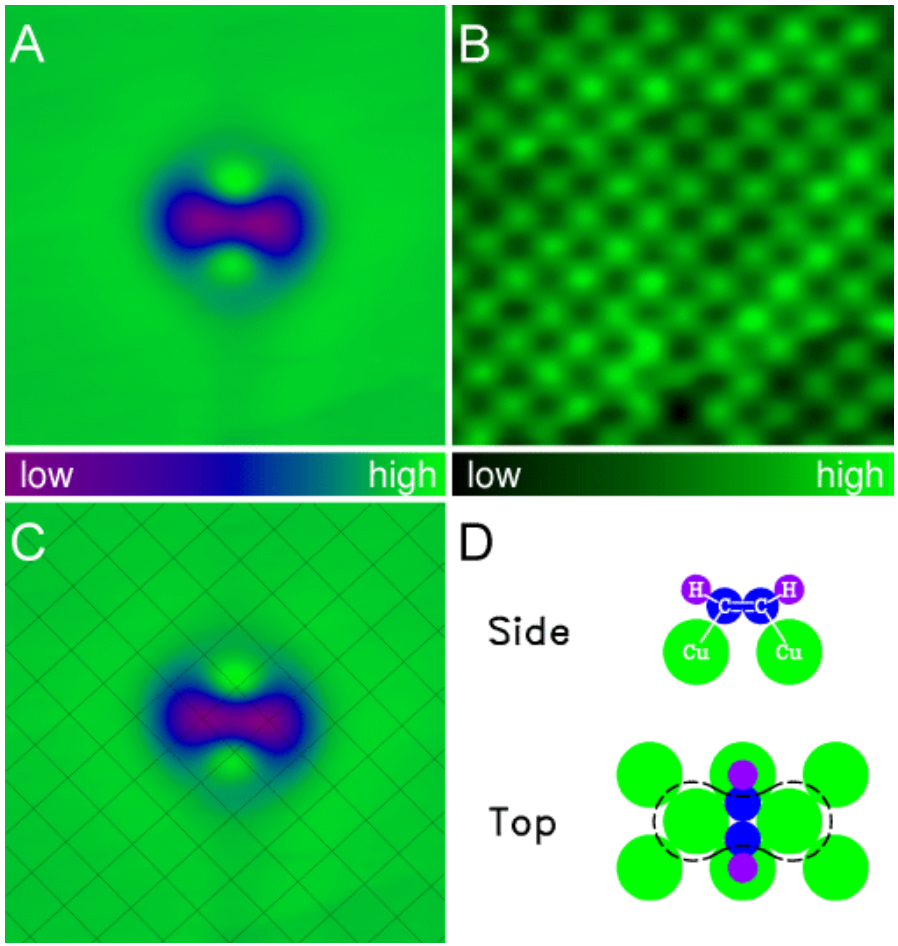

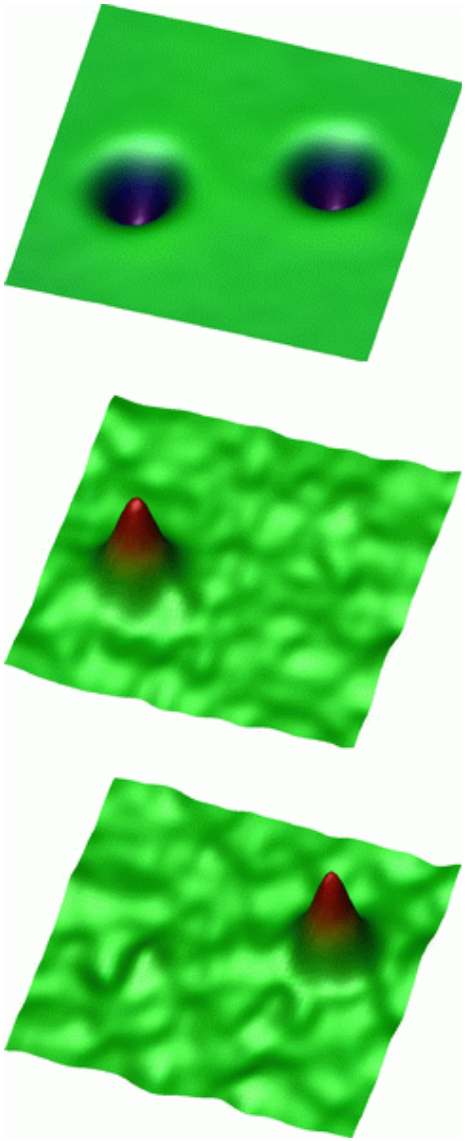

B.C. Stipe, M.A. Rezaei, and W. Ho,
Science **280**, 1732-1735 (1998).

Quantum corral

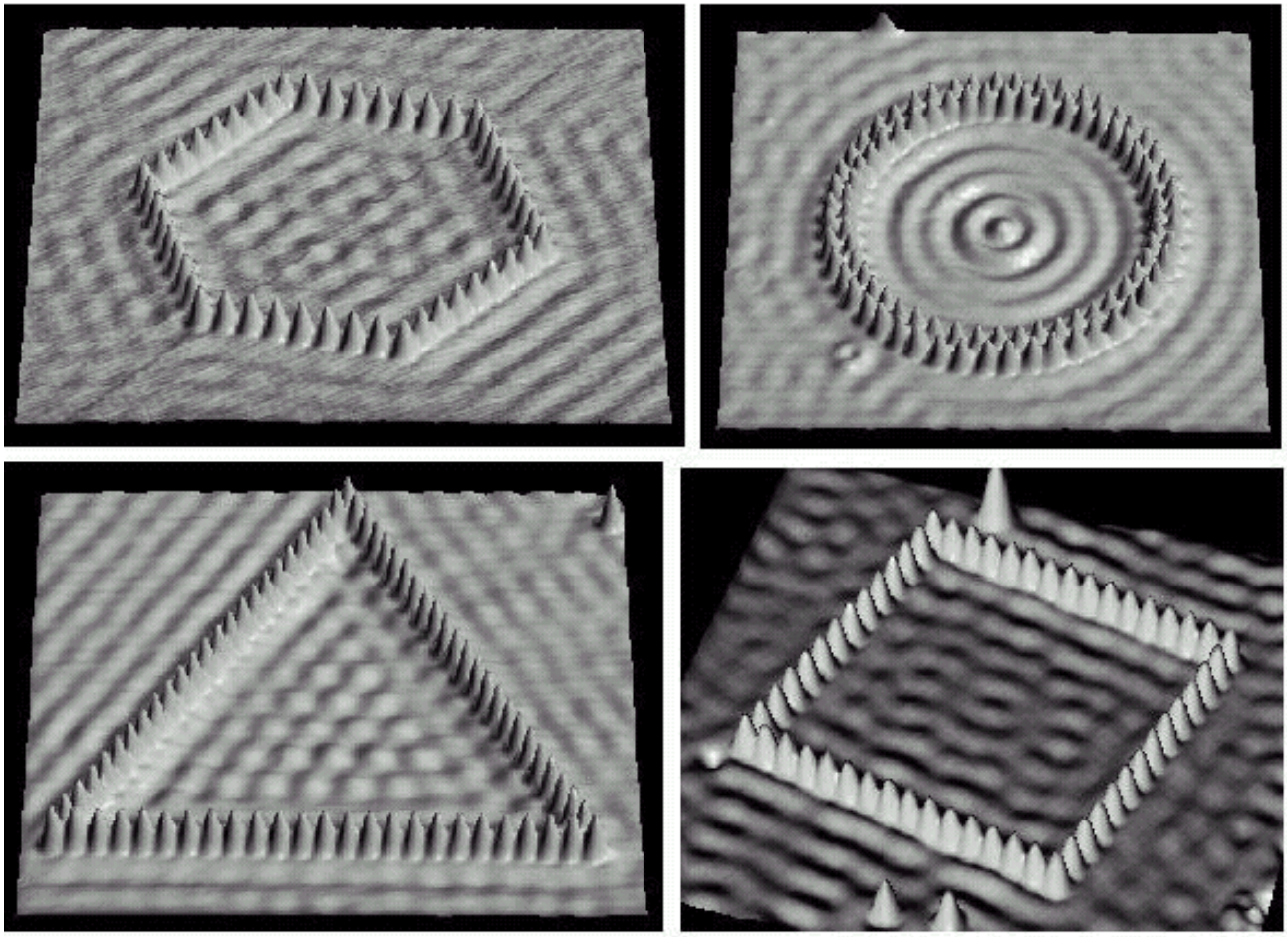

D.M. Eigler, IBM, Amaden

Artificial atom

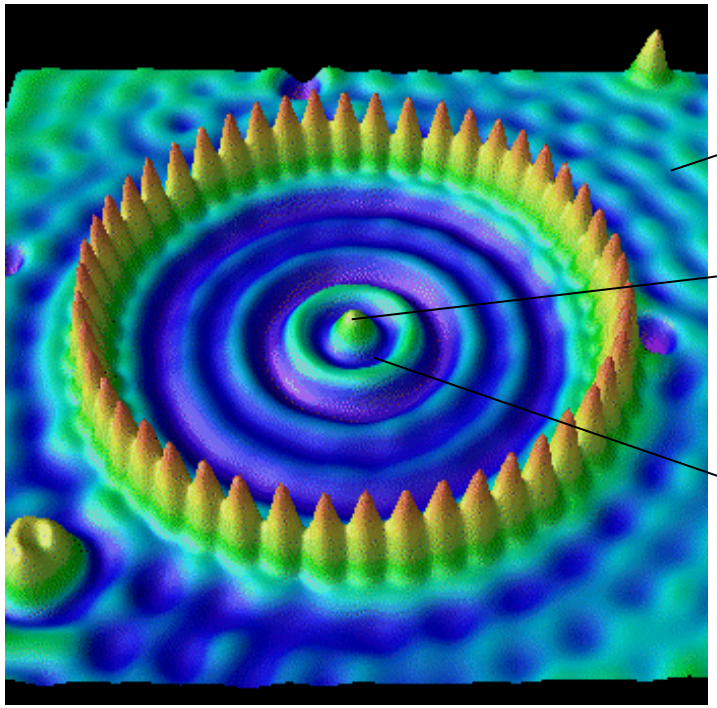

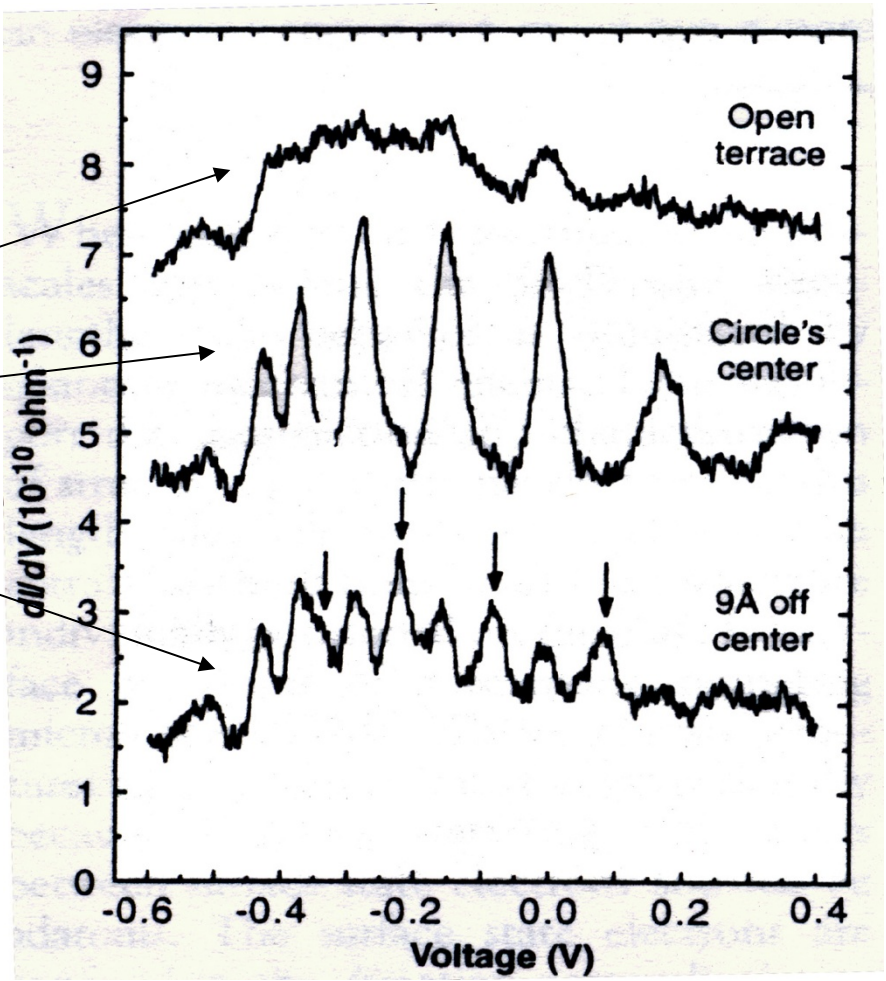

Optical methods with sub-wavelength spatial resolution

Aperture near-field probes

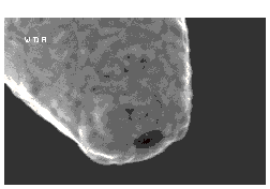

100 nm aperture

Apertureless scattering

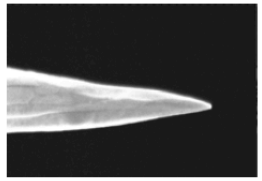

r=20 nm Au tip

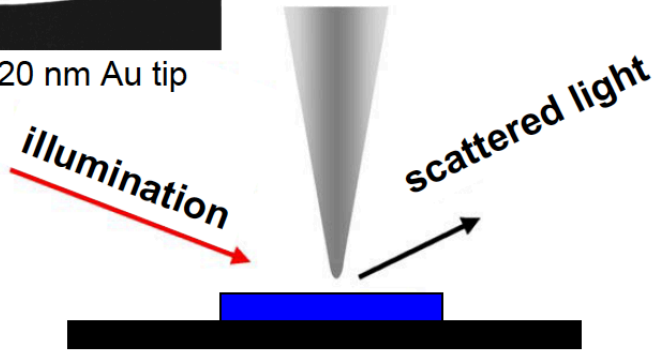

Spatial resolution	**100 nm**	**10 nm**
Time resolution	**100 fs - cw**	**10 fs - cw**
Spectral resolution (cw)	**30 µeV**	**several meV**
Sample temperatures	**10 - 300 K**	**300 K**

Recent development: AFM-IR system

AFM-IR can perform IR spectroscopic chemical identification with sub-100 nm spatial resolution

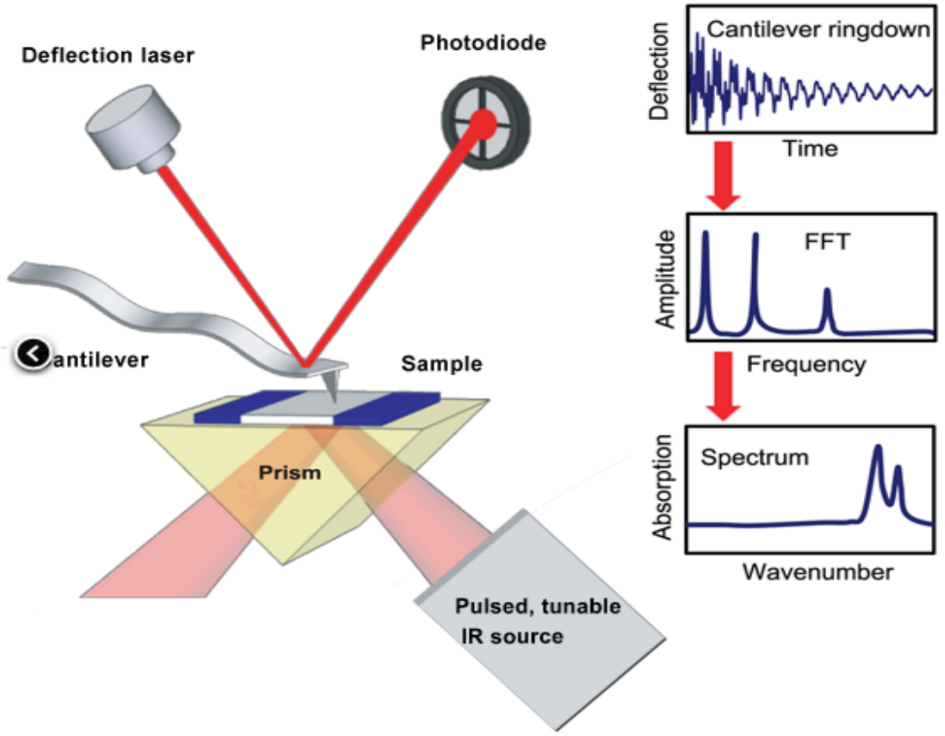

Scheme of the AFM–IR setup. The AFM cantilever ring-down amplitude plotted as a function of laser excitation wavelength produces the IR spectrum.

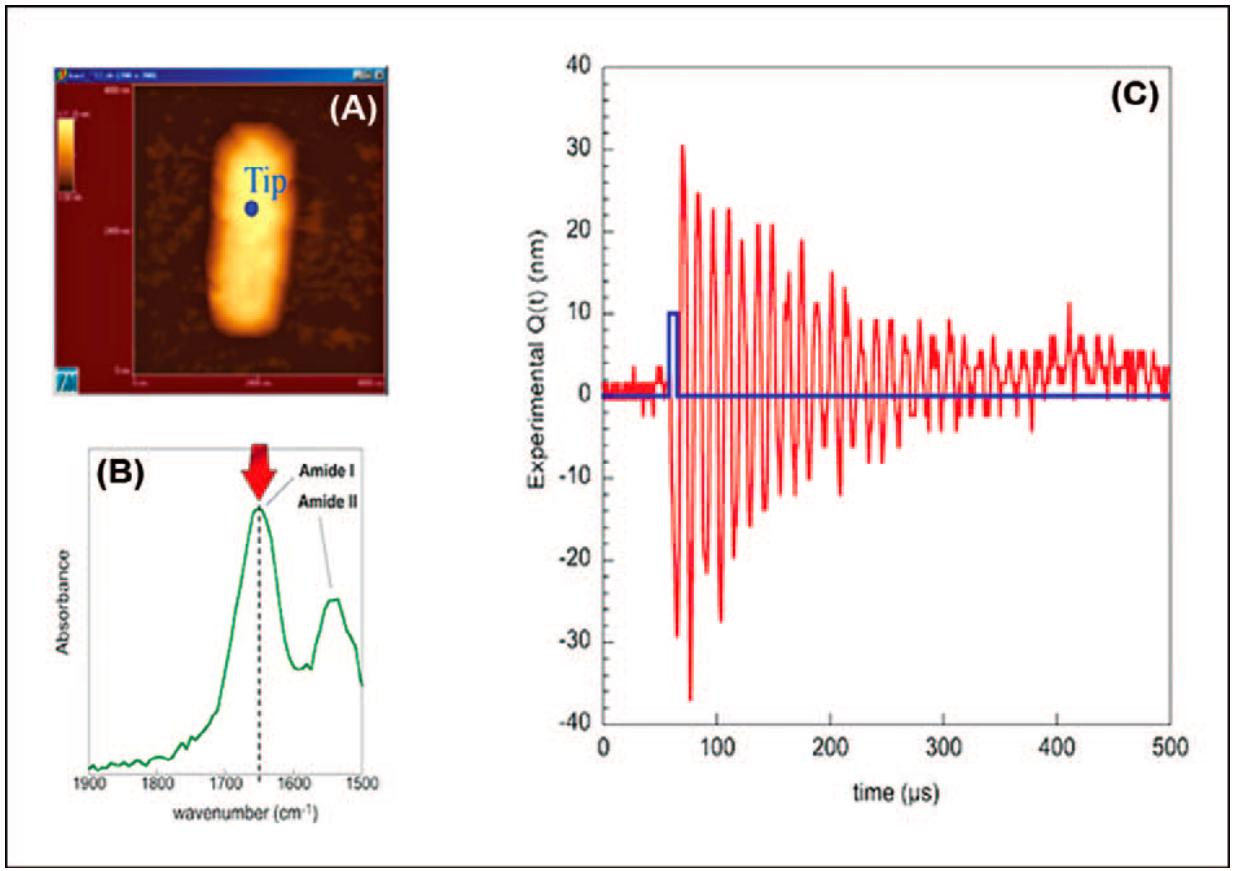

(a) AFM topography picture of the bacterium; the position of the tip is indicated in blue. (b) FT–IR spectrum; the bacterium absorption spectrum is drawn in green, and the wavenumber of the CLIO laser is indicated by the red arrow. (c) Oscillations recorded by the four-quadrant detector (in red) as function of time superposed on the CLIO pulse laser (blue).

Alexandre Dazzi et al., APPLIED SPECTROSCOPY OA 66, 1365 (2012)

Tip-enhanced Raman spectroscopy

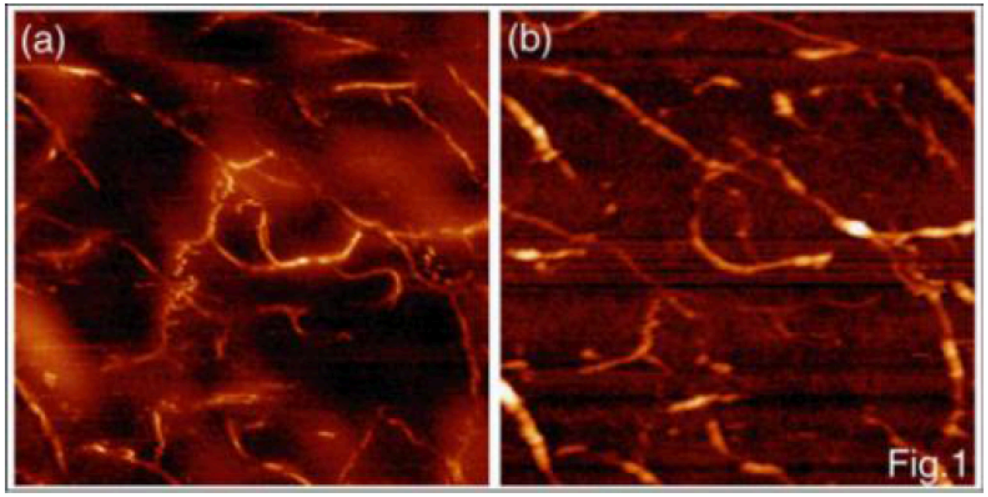

Topography **1594 cm^{-1} vibration**

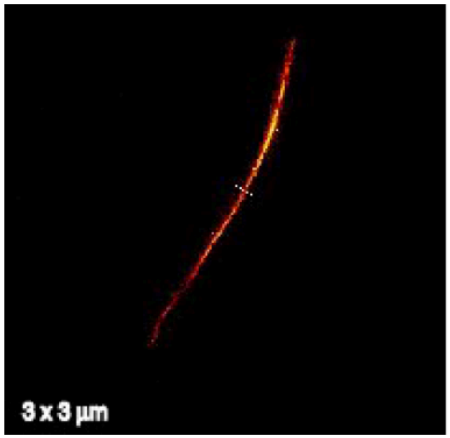

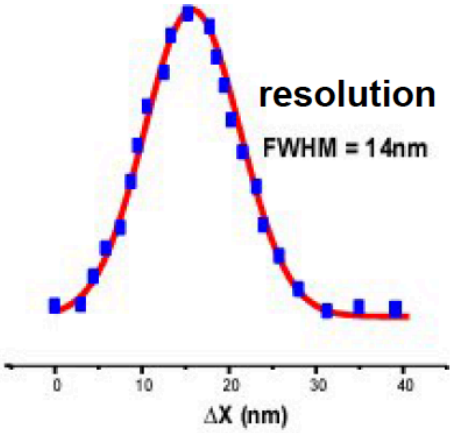

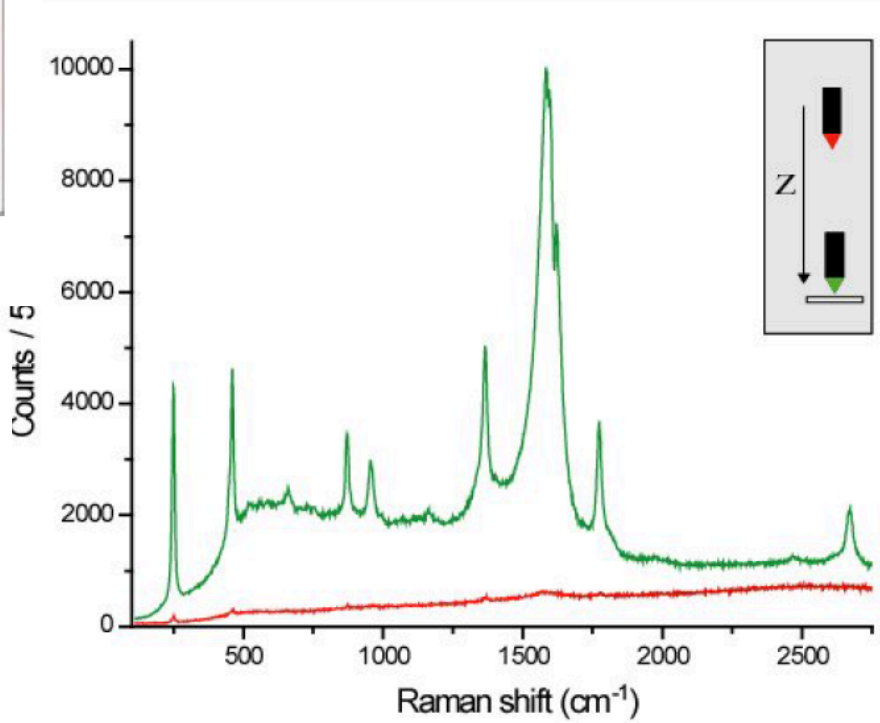

Light scattering from a metallic nanotip

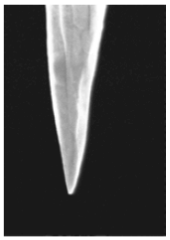

r=10-20 nm

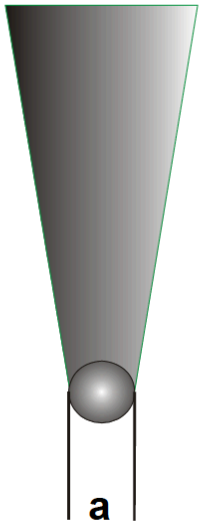

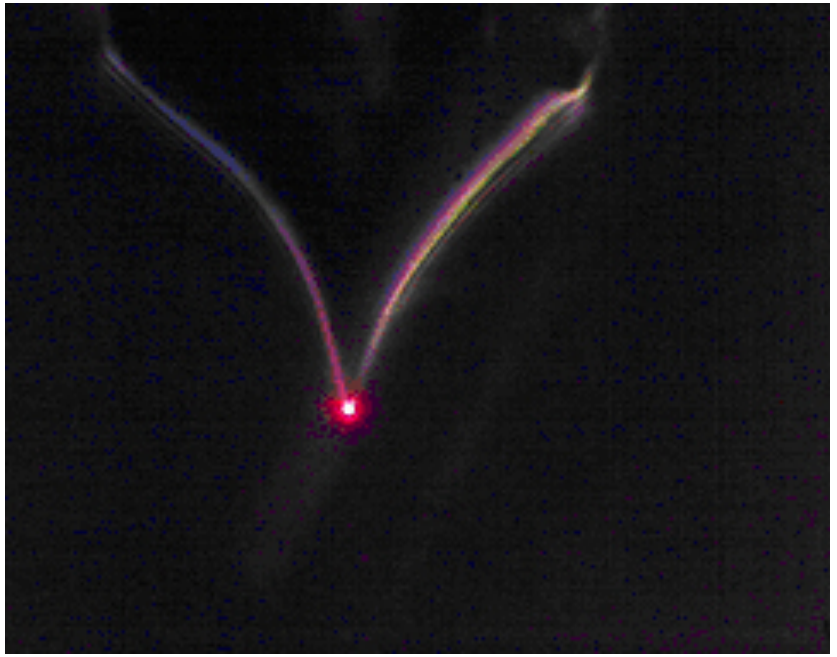

Scatterer dimension a=2r << λ
(Mie scattering)

Electric field enhancement for field vector parallel to tip axis:

- lightning rod effect (field singularity at tip apex)

- surface plasmon excitation

Field enhancement factor 10 – 50

L. Novotny et al., Phys. Rev. Lett. 79, 645 (1997),
Annu. Rev. Phys. Chem. 57, 303 (2006)

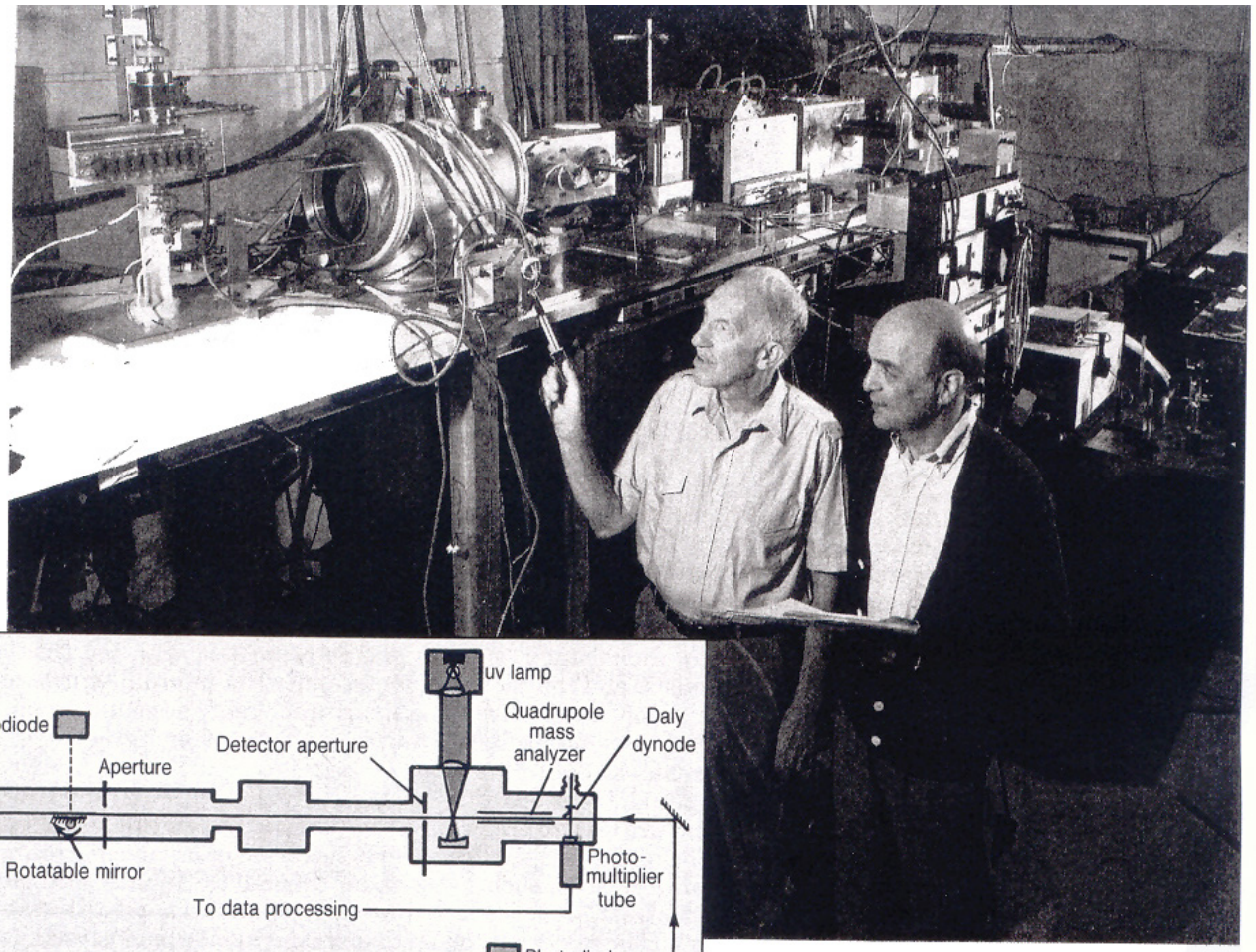

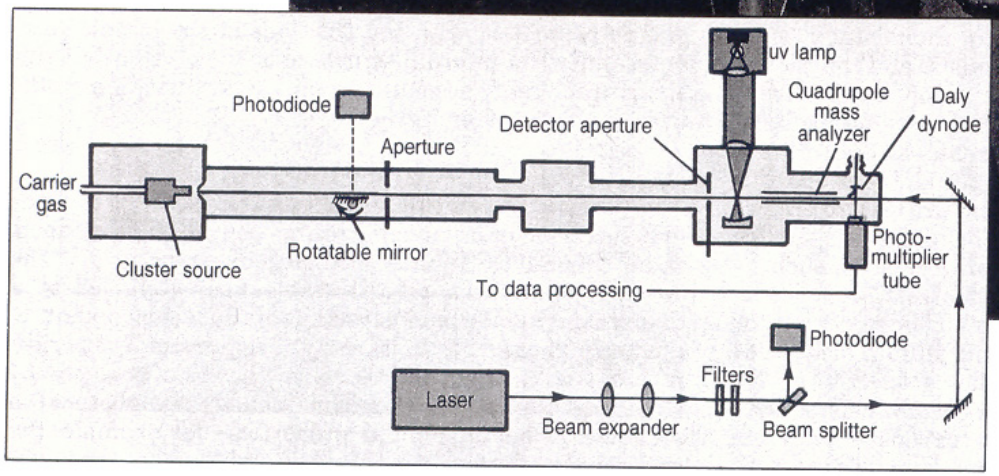
uv lamp
Photodiode
Quadrupole mass analyzer
Daly dynode
Detector aperture
Aperture
Carrier gas
Photo-multiplier tube
Rotatable mirror
Cluster source
To data processing
Photodiode
Filters
Laser
Beam expander
Beam splitter

Mass Analyzer

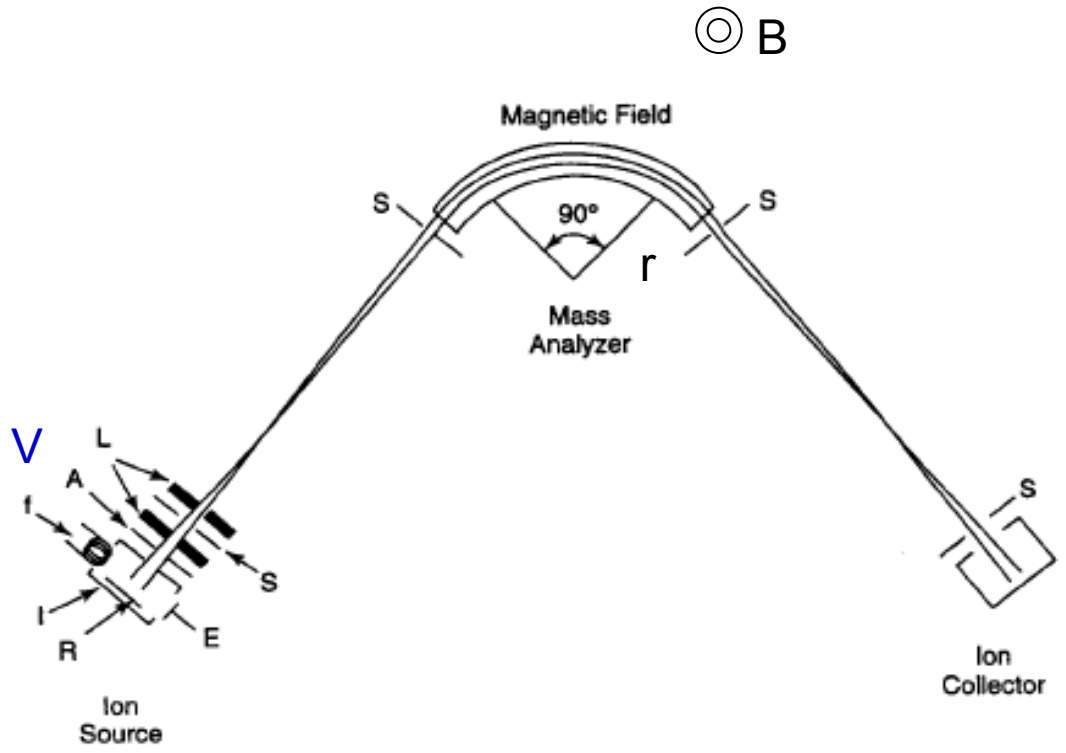

Figure 3.8. Sketch of a mass spectrometer utilizing a 90° magnetic field mass analyzer, showing details of the ion source: A—accelerator or extractor plate, E—electron trap, f—filament, I—ionization chamber, L—focusing lenses, R—repeller, S—slits. The magnetic field of the mass analyzer is perpendicular to the plane of the page.

$qV = \frac{1}{2} mv^2$

$F = qvB = mv^2/r$

$m/q = \frac{1}{2} B^2r^2/V$

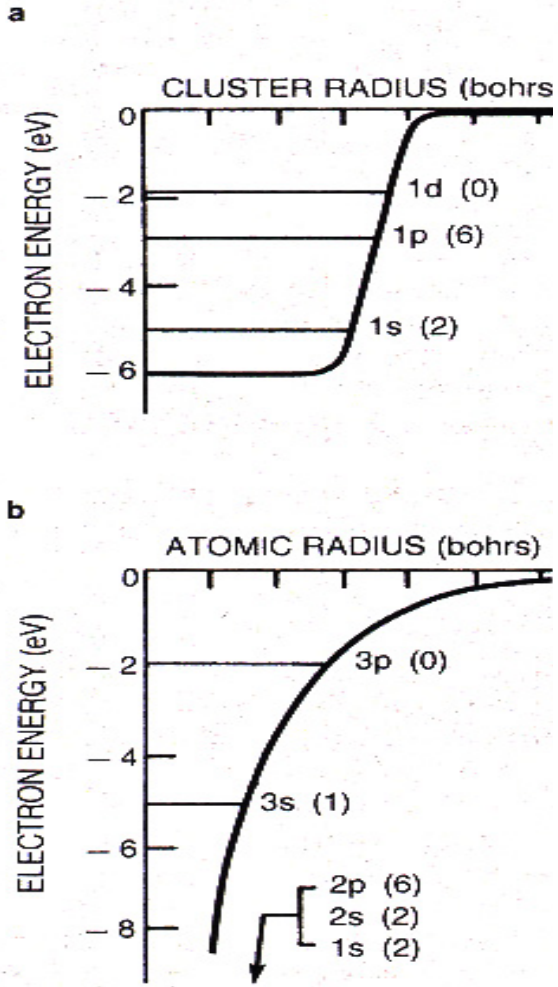

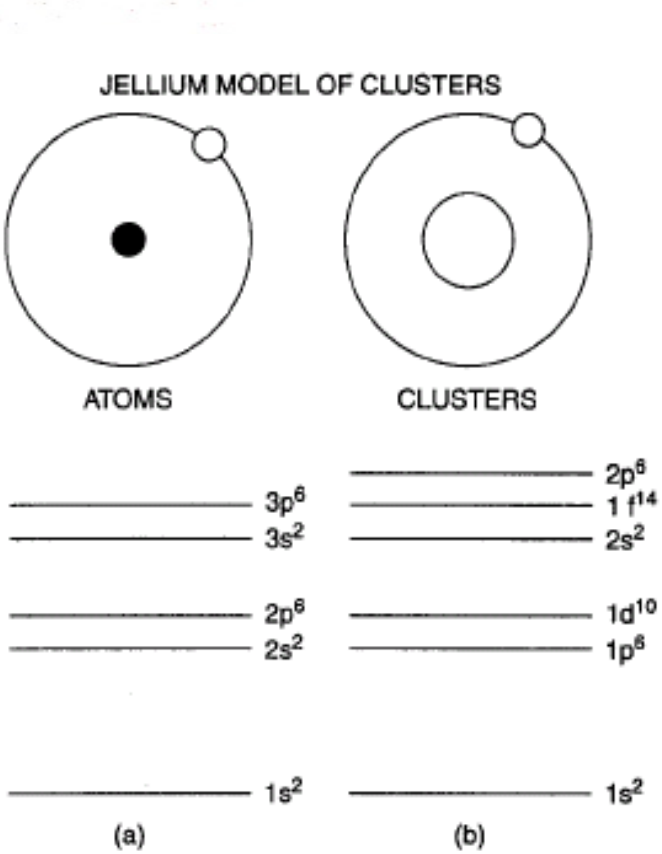

Figure 4.5. A comparison of the energy levels of the hydrogen atom and those of the jellium model of a cluster. The electronic magic numbers of the atoms are 2, 10, 18, and 36 for He, Ne, Ar, and Kr, respectively (the Kr energy levels are not shown on the figure) and 2, 18, and 40 for the clusters. [Adapted from B. K. Rao et al., *J. Cluster Sci.* **10**, 477 (1999).]

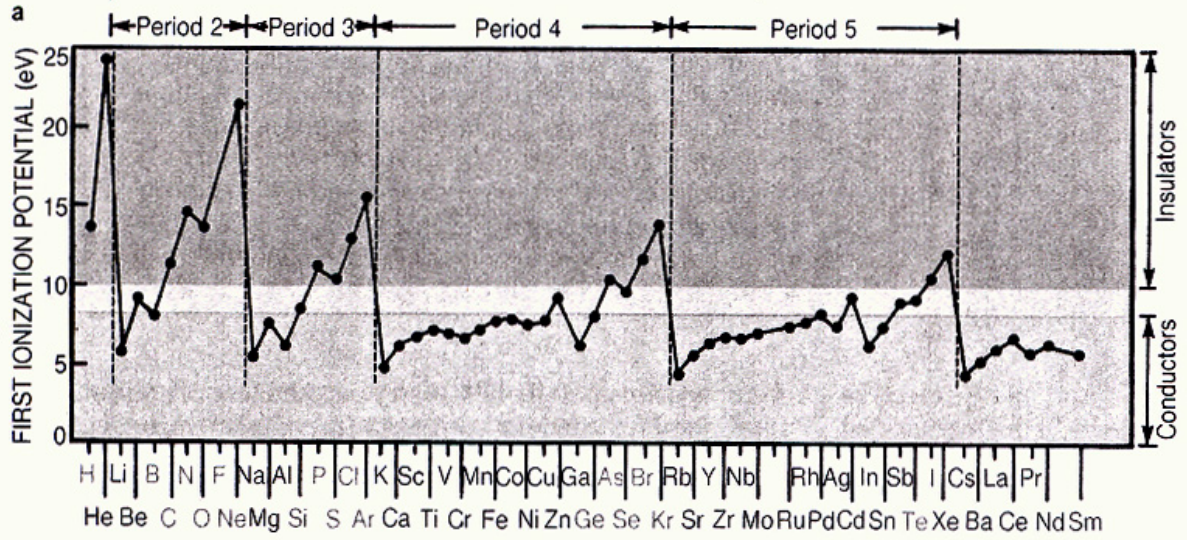

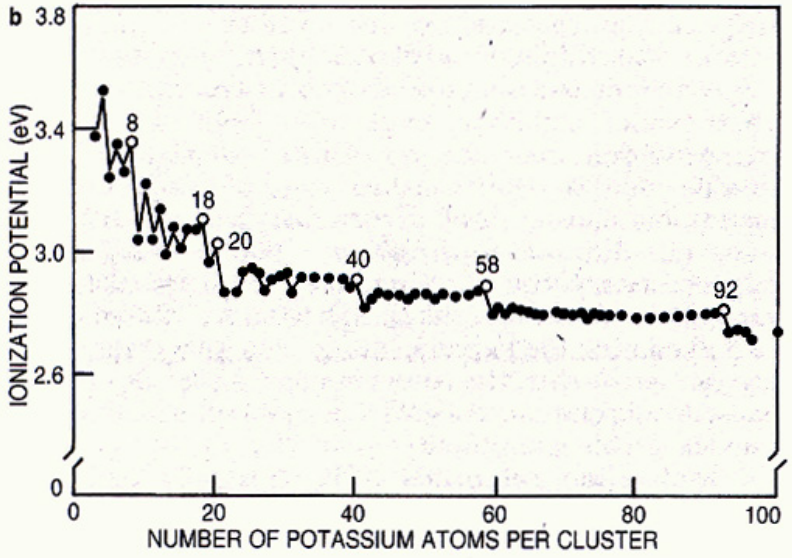

Shell structure: Two views. **a:** Atomic ionization potentials drop abruptly from above 10 eV following the shell closings for the noble gases (He, Ne, Ar and so on). For semiconductors (labeled in blue) the ionization potential is between 8 and 10 eV, while for conductors (red) it is less than 8 eV. It is clear that bulk properties follow from the natures of the corresponding atoms. (Adapted from A. Holden, *The Nature of Solids*, © Columbia U. P., New York, 1965. Reprinted by permission.) **b:** Ionization potentials for clusters of 3 to 100 potassium atoms show behavior analogous to that seen for atoms. The cluster ionization potential drops abruptly following spherical shell closings at $N = 8$, 20, 40 . . . . Features at $N = 26$ and 30 represent spheroidal subshell closings. The work function for bulk potassium metal is 2.4 eV. **Figure 3**

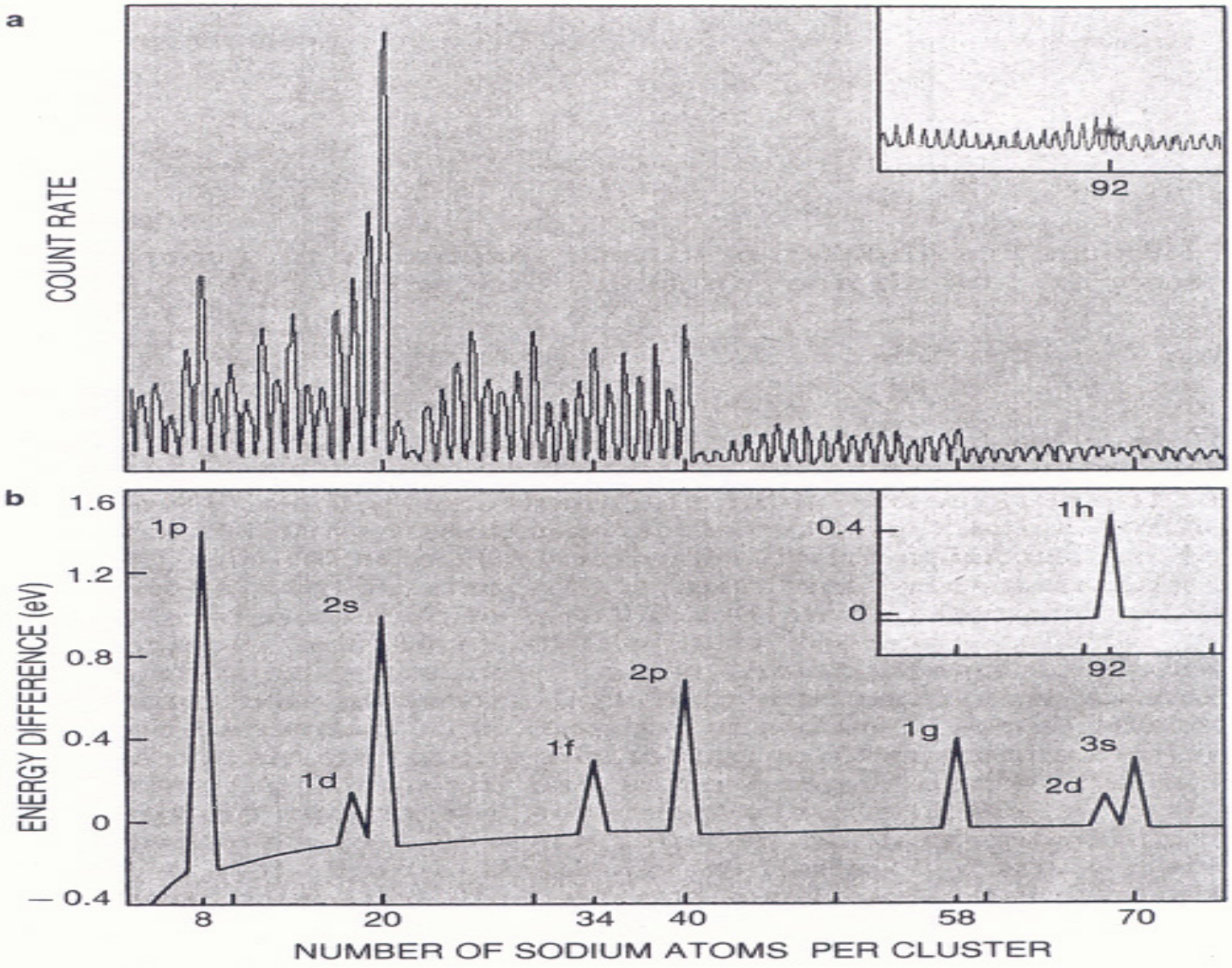
a
COUNT RATE
92
b
ENERGY DIFFERENCE (eV)
1.6
1.2
0.8
0.4
0
−0.4
1p
2s
1d
1f
2p
1g
3s
2d
1h
0.4
0
92
8
20
34
40
58
70
NUMBER OF SODIUM ATOMS PER CLUSTER

Reactivity of nanoclusters

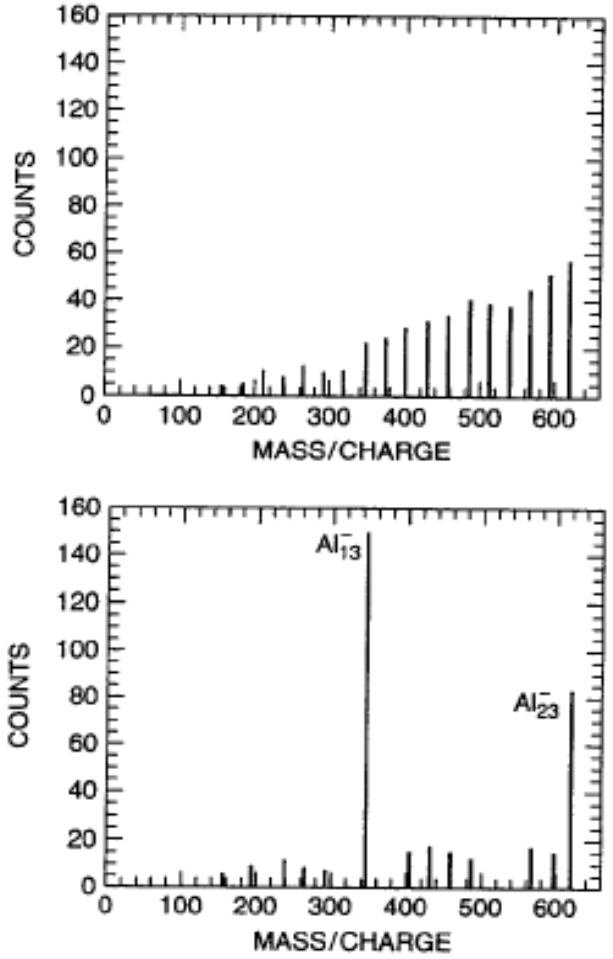

Figure 4.13. Mass spectrum of Al nanoparticles before (top) and after (bottom) exposure to oxygen gas. [Adapted from R. E. Leuchtner et al., *J. Chem. Phys.*, **91**, 2753 (1989).]

Magic clusters

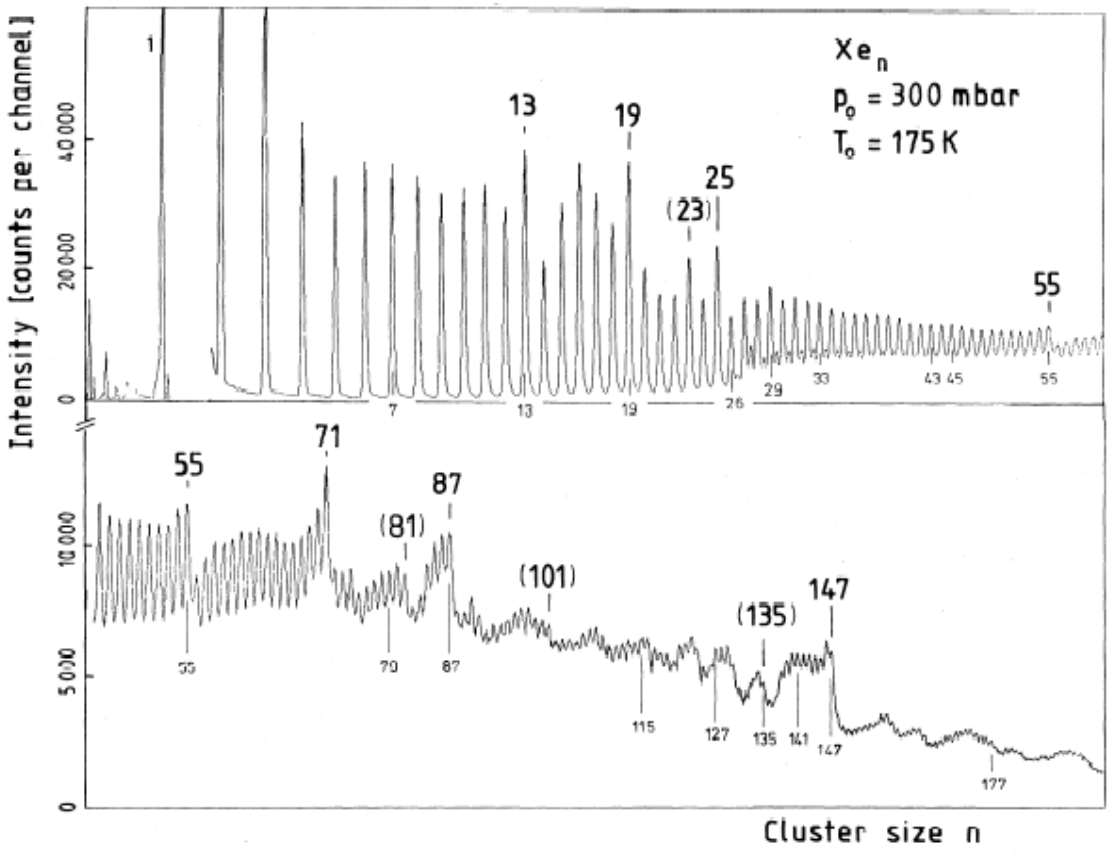

FIG. 1. Mass spectrum of xenon clusters. Observed magic numbers are marked in boldface; brackets are used for numbers with less pronounced effects. Numbers below the curve indicate predictions or distinguished sphere packings.

Mackay icosahedra

P = 1

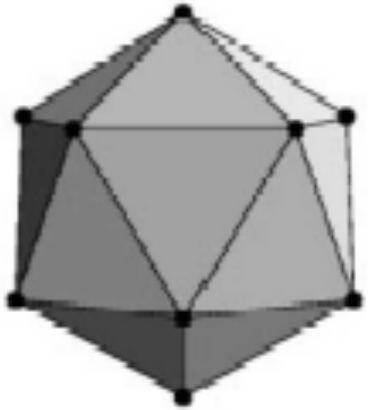

20 fcc(111) faces

P = 2

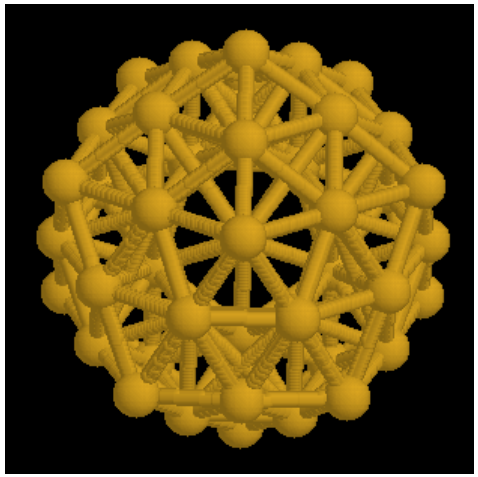

P = 3

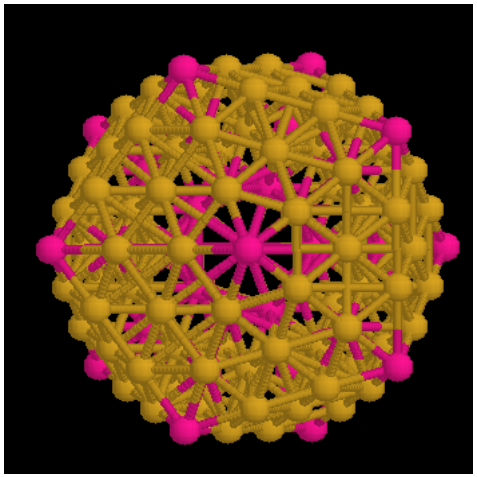

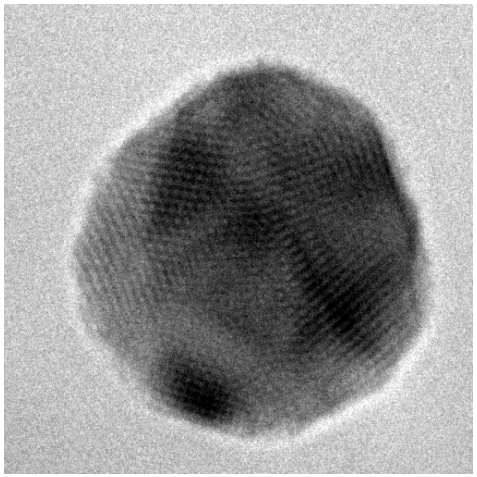

Shell model

$$N = 1 + \Sigma\,(10p^2 + 2)$$